

1 **Rivers, reefs, and deltas; Geomorphological**
2 **evolution of the Jurassic of the Farsund Basin,**
3 **offshore southern Norway**
4

5 Thomas B. Phillips*¹, Christopher A-L. Jackson, Rebecca E. Bell, Ayunda A. Valencia

6 *Basins Research Group (BRG), Department of Earth Science and Engineering, Imperial*
7 *College, South Kensington Campus, Prince Consort Road, London, SW7 2BP, UK*

8 ¹*Now at Department of Earth Science, Durham University, Science Labs, Durham, DH13LE*

9 *Corresponding author: tbphil13@gmail.com

11 **Abstract**

12

13 In many petroleum-bearing, data-poor ‘frontier’ basins, source, reservoir, and seal
14 distribution is poorly constrained, making it difficult to identify petroleum systems and play
15 models. However, 3D seismic reflection data provide an opportunity to directly map the
16 three-dimensional distribution of key petroleum system elements, thereby supplementing
17 typically sparse, one-dimensional sedimentary facies information available from wells. Here,
18 we examine the Farsund Basin, an underexplored basin offshore southern Norway. Despite
19 lying in the mature North Sea basin, the Farsund Basin contains only one well, meaning there
20 remains a poor understanding of its hydrocarbon potential. This E-trending basin is
21 anomalous to the N-trending basins present regionally, having experienced a different
22 tectonic, and likely geomorphological, evolution. We identify a series of east-flowing rivers
23 in the Middle Jurassic, the distribution of which are controlled by salt-detached faults. In the
24 Middle Jurassic, a series of carbonate reefs, expressed as sub-circular amplitude anomalies,
25 developed. Within the Upper Jurassic we identify numerous curvilinear features, which
26 correspond to the downlap termination of southwards-prograding deltaic clinoforms. We
27 show how seismic-attribute driven analysis can determine the geomorphological development
28 of basins, offering insights into both the local and regional tectono-stratigraphic evolution of
29 an area and helping to determine its hydrocarbon potential.

30

31 **1 Introduction**

32

33 Successful hydrocarbon exploration requires a knowledge of how sedimentary basins
34 evolve in terms tectonic events and depositional patterns, and how this leads to the
35 development of working petroleum systems and plays (e.g. Johannessen & Andsbjerg 1993;
36 Posamentier 2004; Dreyer et al. 2005; Holgate et al. 2013). Predicting the occurrence of
37 source, reservoir and source rocks is a critical element of petroleum systems analysis,
38 although this is especially challenging in frontier or underexplored basins due to a lack of
39 well data. Even where available, these well data provide only one- to quasi-three-dimensional
40 constraints on the distribution of various rock types in the subsurface. Outcrop studies may
41 provide detailed insights into the typical geometries and spatial relationships between
42 different facies types, but they do not replicate specific subsurface geometries (e.g. Prélat et
43 al. 2009; Romans et al. 2011; Agirrezabala et al. 2013; Holgate et al. 2014; Legler et al.
44 2014). Therefore, our understanding of the geological complexity of an area, including the
45 distribution of different rock types and constituent petroleum systems, is heavily influenced
46 by well spacing, reducing the accuracy and resolution of derived play maps and tectono-
47 stratigraphic models (e.g. Johannessen & Andsbjerg 1993; Dreyer et al. 2005; Holgate et al.
48 2013; Mannie et al. 2014). These issues are particularly relevant in underexplored areas
49 where a complex area, with a relatively localised geological evolution, may not be
50 incorporated into regional models due to a lack of data and low resolution.

51 High-quality 3D seismic reflection data does not always suffer from such spatial
52 aliasing, providing relatively high-resolution images (10's m) of ancient geomorphic
53 landscapes and seascapes preserved in the Earth's subsurface. By using amplitude and
54 frequency derived seismic attributes, such as root mean square (RMS) amplitude, variance,
55 dominant frequency, and spectral decomposition, we are able to constrain, to varying degrees

56 of confidence, the geometry and distribution of different rocks types within the subsurface
57 (e.g. Ryseth et al. 1998; Posamentier & Kolla 2003; Posamentier 2004; Colpaert et al. 2007;
58 Chopra & Marfurt 2008; Jackson et al. 2010; Zhuo et al. 2014; Klausen et al. 2016; Eide et al.
59 2017). Using 3D seismic reflection data we can therefore examine the stratigraphic evolution
60 of the subsurface over a greater areal extent than borehole data, albeit often at a coarser
61 temporal resolution (e.g. Cartwright & Huuse 2005; Colpaert et al. 2007; Jackson et al. 2010;
62 Jackson & Lewis 2013; Klausen et al. 2016; Saqab & Bourget 2016). Seismic
63 geomorphological analysis can therefore also provide additional context to the geological
64 evolution of an area, helping to reduce exploration risk and to update regional tectono-
65 stratigraphic models in frontier or underexplored areas.

66 Here, we conduct a seismic attribute-driven interpretation of 2D and 3D seismic
67 reflection data located offshore southern Norway, and analyse the 3D facies architecture of
68 the Triassic and Jurassic section preserved in the relatively underexplored Farsund Basin
69 (Figure 1). Data from well 11/5-1, located along the southern margin of the basins, provides
70 independent constraints on the lithology of the depositional elements imaged within the 3D
71 seismic volume (Figure 1). Current paleo-geographical models within this area are largely
72 based on regional borehole-correlation studies, with data primarily from the adjacent
73 Egersund and Norwegian-Danish Basins and little within the Farsund Basin; these studies
74 document a clastic-dominated net-transgressive setting throughout the Jurassic (Sørensen et
75 al. 1992; Mannie et al. 2014; Mannie et al. 2016). However, the tectonic evolution of the
76 Farsund Basin differed to that experienced by adjacent basins, being heavily influenced by
77 activity along the underlying lithosphere-scale Tornquist zone (Phillips et al. 2018). Here, we
78 investigate whether this contrasting tectonic history resulted in a unique stratigraphic record
79 and petroleum systems, unlike those encountered in nearby basins.

80 By undertaking detailed seismic geomorphological analysis and seismic attribute-
81 driven interpretation, we constrain the geomorphological evolution of the Farsund Basin
82 throughout the Jurassic, identifying a series of fluvial systems, carbonate patch reefs and
83 shallow marine deltaic lobes. We compare and contrast our observations of the
84 geomorphological evolution of this area to the regional stratigraphic framework (Figure 1b),
85 providing insights into and further constraining the tectonics, sedimentation history and
86 hinterland character of the basin and wider region.

87

88 **2 Regional geological setting**

89

90 This study focusses on the E-trending Farsund Basin, located offshore southern
91 Norway (Figure 1). To the north and south, the basin is bordered by the Permian-
92 Carboniferous aged Varnes Graben and Norwegian-Danish Basin, respectively (Figure 1)
93 (Heeremans & Faleide 2004; Heeremans et al. 2004), and to the west by the much-explored
94 Permian-Carboniferous Egersund Basin. The structural (e.g. Mogensen & Jensen 1994;
95 Sørensen & Tangen 1995; Jackson et al. 2013; Jackson & Lewis 2013; Tvedt et al. 2013) and
96 stratigraphic evolution (e.g. Sørensen et al. 1992; Mannie et al. 2014; Mannie et al. 2016) of
97 the Egersund Basin has been studied by numerous authors. It is separated from the Farsund
98 Basin by the Stavanger Platform and Lista Nose Fault Blocks (Hamar et al. 1983; Skjerven et
99 al. 1983; Jackson & Lewis 2013; Lewis et al. 2013) (Figure 1). To the east, the Farsund Basin
100 opens into the Norwegian-Danish Basin and Sorgenfrei-Tornquist fault complex (Nielsen
101 2003; Heeremans et al. 2004; Olivarius & Nielsen 2016).

102 The southern margin of the Farsund Basin is defined by the N-dipping Fjerritslev
103 Fault system (Figure 1), which within the 3D seismic volume comprises the Fjerritslev North
104 and Fjerritslev South Faults (Figure 2a). A further E-W striking fault, the Farsund North Fault

105 is located outside of the 3D volume and forms the northern margin to the basin (Figure 1). A
106 series of N-S-striking faults are present across the southern margin of the basin; the two
107 largest of which control the preservation of Triassic strata and are termed NS1 and NS2 to the
108 north and south of the Fjerritslev North Fault, respectively (Figure 2a). At shallower
109 stratigraphic levels, N-S striking faults are largely absent, with the basin morphology
110 controlled by the E-W striking Fjerritslev North and South faults (Figure 2b, c).

111 A detailed analysis of the structural evolution of the Farsund Basin can be found in
112 Phillips et al. (2018), which we here review in the context of the North Sea basin
113 development. Prior to its formation, the proto-Farsund Basin was located along the northern
114 margin of the North Permian Basin, which contained mobile evaporites of the Upper Permian
115 Zechstein Supergroup (Christensen & Korstgård 1994; Heeremans et al. 2004; Jackson &
116 Lewis 2013). The Triassic was associated with regional E-W extension, leading to activity
117 along N-S striking faults, such as NS1 and NS2, across the study area (Figure 2c).
118 Widespread uplift and erosion occurred across large parts of the Central North Sea during the
119 Middle Jurassic in response to uplift of the Mid-North Sea thermal dome (Rathey & Hayward
120 1993; Underhill & Partington 1993). To the east, this resulted in the erosion of Triassic-to-
121 Lower-Middle Jurassic strata and the formation of the BJU across the study area (Figure 3).
122 A regional rift phase is documented across the North Sea from the Late Jurassic-to-Early
123 Cretaceous (Ziegler 1992; Færseth 1996; Coward et al. 2003), which led to the formation of
124 the E-W striking faults, i.e. the Fjerritslev North and South Faults and the Farsund North
125 Fault that define the present-day morphology of the Farsund Basin (Figure 1, 2a) (Mogensen
126 & Jensen 1994; Sørensen & Tangen 1995; Phillips et al. 2018).

3 Dataset and methodology

127
128

129 Seismic interpretation was primarily undertaken on a 500 km² 3D seismic reflection
130 dataset located across the southern margin of the Farsund Basin (Figure 1). These data image
131 to 4 seconds two-way-time (TWT) (c. 6 km) with inline and crossline spacings of 18.75 m
132 and 12.50 m, respectively. Frequency values were measured throughout the interval of
133 interest (0.75-1.30 s TWT) and range from 25-40 Hz, with a mean frequency of ~35 Hz
134 (Figure 4). Using an average velocity of 2.5 kms⁻¹ for the overlying sedimentary cover
135 (based on well 11/5-1), corresponding values of vertical resolution ($\lambda/4$) range from 15 to 25
136 m (Figure 4a). Based on an average frequency of ~35 Hz we determine an average vertical
137 resolution ($\lambda/4$) of ~18 m and an average limit of detectability ($\lambda/30$) of ~2 m (Widess 1973;
138 Kallweit & Wood 1982; Slatt 2006).

139 Additional seismic interpretation was undertaken on a series of N-S oriented 2D
140 seismic sections (Figure 1), which image to 7 s TWT (c. 15 km) and allow interpretation of
141 the stratigraphic horizons over a wider area, providing a more regional perspective to our
142 interpretations. Seismic data are displayed as zero phase and follow the SEG normal polarity
143 convention; that is, a downward increase in acoustic impedance is represented by a peak
144 (black), and a downward decrease in acoustic impedance is represented by a trough (red)
145 (Figure 3). The ages of key stratigraphic horizons are constrained through a number of wells
146 regionally (Figure 1). Well 11/5-1, the only well located within the 3D seismic volume
147 (Figure 2), provides detailed 1D facies information within the study area and is tied to the
148 seismic interpretations through a seismic-well tie (Figure 5). The synthetic seismogram
149 proves a good fit to the seismic data in areas where both sonic and density logs are available,
150 with a good match between the top Rotliegend and top Sandnes horizons, and the lower
151 section of the Egersund Formation (Figure 5). There is a poor fit throughout the Egersund and

152 Tau Formations that is primarily related to a lack of density log information in the interval
153 1130-1180 m. Areas immediately above and below this data-absent interval, and towards the
154 top of the log, where data recording begins, are influenced by edge effects relating to data-
155 absent areas and therefore poorly correlate with the original seismic trace (Figure 5). Seismic
156 attributes, such as RMS amplitude, variance, dominant frequency, and spectral decomposition
157 were calculated within windows located either above, below or between specific key horizons
158 in order to further interrogate and extract information from the seismic data (see Appendix A
159 for details regarding specific seismic attributes).

160 We used GeoTeric software in order to calculate the spectral decomposition attribute.
161 To do this, we extracted a frequency spectrum from the data and split this into a series of
162 discrete bins, each corresponding to a range of 10 Hz (Figure 4). Frequency values centred on
163 22, 30 and 45 Hz were assigned to the colours red, green and blue, respectively and blended
164 to produce the spectral decomposition attribute (Figure 4b).

165

166 **4 Regional stratigraphy**

167

168 We here describe the stratigraphic succession preserved in the Farsund Basin as
169 revealed by well 11/5-1, and compare it to the succession encountered regionally (Figures 1,
170 2, 5). The Triassic interval is non-marine succession across the much of the North Sea
171 (McKie & Williams 2009; Jarsve et al. 2014). Triassic strata are preserved within the
172 footwalls of the NS1 and NS2 faults, although no Triassic strata are encountered in well 11/5-
173 1, with Middle Jurassic strata unconformably overlying the Upper Permian Rotliegend Group
174 due to erosion by the BJU (Figure 3, 5). The Middle Jurassic (Bajocian-Bathonian) Bryne
175 Formation is present regionally, but is also not present in well 11/5-1 (Figure 5). The Bryne
176 Formation in the adjacent Egersund Basin comprises non-marine sandstone and siltstone

177 (Vollset & Doré 1984; Mannie et al. 2016). Stratigraphically above the Bryne Formation, and
178 forming the lowermost Jurassic interval penetrated in well 11/5-1, is the Mid-Jurassic
179 (Callovian) Sandnes Formation. In well 11/5-1 this is comprised of 45 m of predominantly
180 marine sandstones and mudstones, with some intervals containing abundant m-scale
181 carbonate stringers (Figure 5) (Vollset & Doré 1984; Mannie et al. 2016). The Late
182 Callovian-to-Early Tithonian Egersund and Tau formations are situated stratigraphically
183 above the Sandnes Formation. These formations make up the majority of the Jurassic interval
184 in well 11/5-1 (189 m) and consist of organic-rich claystones and shales (Figure 5). Isolated
185 glauconitic and pyritic layers are present throughout these formations, indicating a low-
186 energy depositional environment that was prone to anoxic conditions (Figure 5) (Vollset &
187 Doré 1984). Regionally, the uppermost Jurassic (Tithonian) to lower Cretaceous Sauda
188 Formation consists of marine shales. However, in well 11/5-1, the upper 15 m of the 22 m
189 thick Sauda Formation (incorporating the lowermost Lower Cretaceous interval) is
190 sandstone-dominated (Figure 5). The Jurassic interval in both the Farsund Basin and
191 regionally is overlain by a large thickness of Lower Cretaceous deepwater claystones and
192 mudstones.

193

194 **5 Seismic geomorphological observations and interpretation**

195

196 Well 11/5-1 provides direct constraints, albeit only in one dimension, on the
197 stratigraphy of the Triassic and Jurassic succession of the Farsund Basin. Using this
198 stratigraphic framework, we now use a suite of seismic attributes (see Appendix A) to
199 determine the 3D geometry and distribution of different facies types within the basin. In each
200 subsection, we first describe our seismic geomorphological observations, based on seismic
201 reflection, seismic attribute and well data analysis before posing an interpretation for the
202 likely depositional environment and geomorphological origin of the identified features.

203 **5.1 Triassic – Limit of thin-skinned tectonics and depositional extent of mobile** 204 **Zechstein salt**

205

206 In the North Permian Basin, Zechstein salt is overlain by Triassic strata (Clark et al.
207 1998; Lewis et al. 2013). Post-depositional salt mobilisation and modification means that the
208 initial depositional limit of salt and salt basins is often uncertain (Clark et al. 1998; Jackson &
209 Lewis 2013). Triassic strata in the Farsund Basin are dominated by S-dipping, salt-detached
210 normal faults, related to southwards directed salt-mobilisation into the Norwegian-Danish
211 Basin (Figure 6). The top of the Triassic interval is eroded by the BJU, with Triassic strata
212 largely absent across the footwalls of NS1 and NS2, north of the Fjerritslev South Fault
213 (Figure 3, 5). The Fjerritslev North and South Faults in this area do not show any pre-
214 Cretaceous activity and were not present during the Triassic, with the Fjerritslev South Fault
215 appearing restorable up to the BJU (Figure 3, 6) (Phillips et al. 2018).

216 Within the hanging wall of the Fjerritslev South Fault, a series of small-scale (c. 50
217 ms TWT, 70 m height) clinoforms are identified in the Triassic interval, prograding towards
218 the south (Figure 6). The relatively small height of these clinoforms, and the sub-aerial
219 regional character of the Triassic (Jarsve et al. (2014), implies deposition within a terrestrial,

220 likely fluvio-deltaic environment (cf. Patruno et al. 2015a). Immediately south of these
221 clinoforms, now located on the footwall of the Fjerritslev South Fault, thin-skinned salt-
222 detached faulting is restricted northwards (Figure 6). We propose that the transition from the
223 preserved clinoform sequence in the north, to where the clinoforms are bisected by thin-
224 skinned salt-related faults in the south could indicate the initial northern depositional limit of
225 the mobile component of the Zechstein salt (Figure 6). North of this limit, mobile Zechstein
226 salt, or salt of sufficient thickness to flow, is not present. We propose the following model;
227 prior to salt mobilisation, deltaic clinoform sequences prograded southwards over the
228 Zechstein salt basin (Figure 6). Following the onset of salt mobilisation during the Triassic,
229 areas with underlying Zechstein salt were subject to the formation of thin-skinned salt-
230 detached faults, offsetting shallower strata, including the clinoform sequence. However, areas
231 north of the initial depositional limit, where no salt was present or was unable to flow, were
232 unaffected and preserve the southwards prograding clinoform-bearing sequences (Figure 1,
233 6). Using these criteria we are able to map the original depositional limit of mobile Zechstein
234 salt across the present-day Farsund Basin. The depositional limit strikes E-W across the
235 footwall of the Fjerritslev South Fault, which had not formed at that time (Figure 1). Further
236 east, the depositional limit of the Zechstein salt steps northwards across NS2, indicating that
237 some relief may have been present across this fault during salt deposition, before continuing
238 in an E-W orientation to the east (Figure 1).

239 **5.2 Bryne Formation – Fluvial systems**

240

241 In the footwall of the Fjerritslev South Fault we identify two high-amplitude, laterally
242 discontinuous reflections above the BJU (Figure 7). Additional features may be present
243 elsewhere in the basin, but are not identifiable due to overall high reflectivity through much
244 of this succession. The high-amplitude reflections are situated in the hanging walls of thin-
245 skinned, salt-detached faults (Figure 7). Each feature is around 500 m wide and is imaged as

246 a very high-amplitude, tuned seismic reflection, making it difficult to calculate their true
247 thickness (Figure 3, 7) (Widess 1973; Brown 2011). However, given that the vertical
248 resolution of the data in this interval is ~24 m (Figure 4a), this value represents a maximum
249 thickness estimate. Due to the restricted lateral extent of these reflections, and their
250 stratigraphic position below the Sandnes Formation, we interpret these features are not
251 penetrated by well 11/5-1 and instead correspond to the Bryne Formation, thereby
252 representing the oldest Jurassic strata in the Farsund Basin.

253 We extract RMS amplitude, variance and dominant frequency seismic attributes,
254 calculated within a 25 ms TWT window above the top of the BJU horizon in order to
255 encompass the full thickness of the features, highlight their 3D geometry and provide clues as
256 to their geological origin (Figure 7). In map view, the RMS amplitude attribute highlights two
257 E-W trending high-amplitude features, with curvi-linear channel-like geometries, on the
258 footwall of NS2, termed Channel 1 and Channel 2 from north to south, respectively (Figure
259 8). Channel 1 is ~8 km long and can be traced westwards across the footwall of the Fjerritslev
260 South Fault. It is not imaged in the hanging wall of the Fjerritslev South Fault, due to the
261 amplitude signal being masked by higher background amplitudes (Figure 8). Channel 2
262 originates within the footwall of the Fjerritslev South Fault, has an overall length of ~9 km,
263 and widens eastwards from c. 200 m to c. 400 m (Figure 8). In cross-section the channels
264 display an asymmetric geometry, with Channel 2 being thicker towards the south (Figure 7).
265 Both channels cross, and are not offset by, NS2 to the east (Figure 8). However, the channels
266 widen as they cross NS2, from c. 500 m in the footwall to c. 2 km in the hanging wall.
267 Furthermore, the channels display a more SE orientation within the footwall of the fault
268 (Figure 8).

269 The variance and dominant frequency seismic attributes provide more detailed
270 insights into the channel geometry. The variance attribute highlights a series of minor linear

271 channels oriented perpendicular to, and joining along both channel 1 and 2. These secondary
272 channels display lengths and widths of ~400 m and ~150 m, respectively (Figure 8c). In some
273 instances these minor channels link Channel 1 and Channel 2 ('linking channel' on Figure
274 8e). The secondary channels display an asymmetric distribution with respect to the main
275 channel, being concentrated along one margin, which displays a relatively shallow gradient.
276 The opposite margin of the channel is more sharply defined and is often associated with an
277 underlying salt-detached fault (Figure 7, 8). The dominant frequency attribute further defines
278 the first-order geometry of the channels within the footwall of NS2, which are delineated by
279 relatively high frequencies (~45 Hz along the margins of the channels and ~35 Hz in the
280 centre).

281 Based on the seismic attribute-derived observations described above, we interpret
282 these channel-like features as originally E- to SE-flowing, Middle Jurassic fluvial systems
283 within the Bryne Formation. The high-amplitude character of the channels indicates a
284 different, perhaps more sand-prone, lithology to the Egersund and Sandnes formation
285 mudstone above and potentially fine-grained lithologies below (Figure 5, 7). The smaller
286 structures merging along the margins of the main channels are interpreted as tributaries
287 (Figure 8e). The E-W orientation of the channels is partly controlled by underlying thin-
288 skinned, salt-detached faults. The underlying faults appear associated with a more sharply-
289 defined channel margin that hosts a few tributaries, whereas the adjacent margin is associated
290 with a gentler gradient and hosts numerous tributaries (Figure 8e). This asymmetric geometry
291 indicates that, at least in the west, movement along these thin-skinned faults influenced the
292 depositional surface and channel physiography. The channels were unaffected by the
293 Fjerritslev South Fault, as this was not present at the time. Towards the east the channels
294 widen across a topographic gradient located above NS2. This topographic gradient formed
295 due to differential compaction of Triassic strata across the now inactive fault (Figure 8). The

296 widening of the channels appears to represent an estuarine setting, transitioning from a non-
297 to shallow-marine environment. This indicates that the location of NS2 likely represented the
298 paleo-shoreline during the deposition of the Bryne Formation in the Middle Jurassic.

299 **5.3 Sandnes Formation – Patch reef development**

300

301 Atop the Bryne Formation channel systems, a series of isolated high-amplitude
302 features (IHAFs) are identified within a stratigraphic interval corresponding to the Middle
303 Jurassic Sandnes Formation, which overlies the BJU and, where present, the Bryne
304 Formation. As penetrated in well 11/5-1, the Sandnes Formation consists of sandstone and
305 mudstone, with some isolated carbonate stringers also present. No IHAFs are directly
306 penetrated by the borehole (Figure 5).

307 In cross-section, the IHAFs display a double (peak-trough) reflection character, with a
308 large positive impedance contrast at the top (Figure 9). Two distinct IHAF morphologies are
309 identified; short, wide structures with heights of 25 ms TWT (c. 30 m), and taller, narrower
310 structures with typical heights of 35 ms TWT (c. 50 m) (Figure 9). The plan-view
311 morphology of the IHAFs is further highlighted by seismic attributes (Figure 10). RMS
312 amplitude, variance and dominant frequency attributes were extracted from a 50 ms window
313 above the BJU and also above the Bryne Formation channels, ensuring coverage of the full
314 height of the structures and a lack of input from stratigraphically lower features. In map-view
315 the IHAFs are expressed as circular to sub-circular high amplitude anomalies, consisting of a
316 high amplitude core and relatively low amplitude margin (Figure 10). A total of 333 IHAFs
317 are identified across the area; smaller IHAFs are most accurately delineated using the spectral
318 decomposition attribute (Figure 10c). The larger structures have a diameter of c. 450 m;
319 whilst the smaller structures have a diameter of c. 150 m (Figure 9, 10). The tall, narrow
320 IHAFs are predominately situated within the hangingwall of NS2, whereas the short, wide

321 IHAFs are restricted to the footwall (Figure 10d). Notably, the distributions of the two
322 different morphologies are unaffected by the E-trending Fjerritslev North and Fjerritslev
323 South faults that dominate the present-day basin morphology but were not present during the
324 deposition of the Sandnes Formation with the wider, shorter IHAFs situated on both the
325 hanging walls and footwalls of the Fjerritslev North and South faults (Figure 10). The
326 distribution of the IHAFs does not change laterally to the south and west, indicating that the
327 IHAF domain may extend outside of the 3D volume. However, the concentration of the
328 IHAFs does decrease to the NE, in the hanging wall of both NS2 and the Fjerritslev North
329 Fault, implying that this may represent a limit to the IHAF domain (Figure 10).

330 In some instances the IHAFs are cross-cut by later faults (Figure 10d, f), implying that
331 they are brittle in nature. Some IHAFs display non-rounded, more elongate geometries,
332 which RMS amplitude shows is typically a result of these IHAFs containing multiple high
333 amplitude nuclei. The typical sub-rounded morphology of the IHAFs implies a radial mode of
334 growth, with those IHAFs that contain multiple nuclei representing IHAFs that have grown
335 radially and since merged (Figure 10e).

336 A variety of different processes can lead to the formation of sub-circular structures in
337 seismic reflection data (Stewart 1999), including volcanic edifices (both igneous and mud-
338 related) (Davies & Stewart 2005), hydrothermal vent systems (Magee et al. 2016), gas
339 accumulations and pockmarks (Hovland et al. 1987; Fichler et al. 2005; Andresen et al. 2011;
340 Agirrezabala et al. 2013; Marcon et al. 2014), carbonate reefs (Posamentier & Laurin 2005;
341 Rosleff-Soerensen et al. 2012; Saqab & Bourget 2016) and evaporite structures (Jackson &
342 Talbot 1986). Based on the relatively small (100's m scale) scale of the structures, coupled
343 with a lack of igneous activity within this area at this time, we discount an igneous/volcanic
344 edifice related origin for the IHAFs. Similarly, the small-scale of the IHAFs, and the lack of
345 regional igneous activity also discounts an origin as hydrothermal vent systems (Magee et al.

2016). In addition, we do not consider an evaporate-related origin based on the IHAFs being located stratigraphically above the Upper Permian Zechstein salt, and there being no Jurassic salt present in this area of the North Sea (Jackson & Lewis 2013). Furthermore, the IHAFs are also present north of the aforementioned depositional limit of the Zechstein salt (Figure 1, 6). The relatively small-scale nature of the structures would be consistent with an origin as pockmarks; however, the structures are associated with positive relief whereas pockmarks would typically form cavities infilled with material from overlying strata (Hovland et al. 1987; Agirrezabala et al. 2013; Kluesner et al. 2013; Marcon et al. 2014).

Therefore, based on: i) their radial growth mode; ii) the positive impedance contrast at the top of the structures; iii) their overall size and morphology, along with the binary nature of the size distribution potentially reflecting different growth conditions; and iv) their brittle nature, we interpret that the IHAFs represent a series of carbonate patch reefs. Carbonate is present locally, as demonstrated by the carbonate-rich intervals penetrated in well 11/5-1 (Figure 5). Modern-day carbonate patch reefs are typically found within shallow marine environments and are often associated with sheltered low-energy environments. Modern patch reefs have diameters of c. 200 m, and heights of c. 10 m, similar to those within the study area (e.g. Brock et al. 2008; Purkis et al. 2015). The binary size distribution of the IHAFs may reflect growth conditions in slightly different, albeit still shallow, water depths. The IHAFs in slightly deeper water grow preferentially upwards towards the sea surface, compared to the wider, shorter patch reefs located in shallower waters, which have limited accommodation space and therefore grow laterally (Kendall and Schlager 1981; Schlager 1981). Carbonate patch reefs have previously been identified on seismic reflection data, displaying similar geometries, morphologies and seismic character to the IHAFs identified here (Posamentier & Laurin 2005; Ruf et al. 2008; Rosleff-Soerensen et al. 2012; Saqab & Bourget 2016). No larger-scale atolls or barrier reefs are identified in the Farsund Basin,

371 unlike in other examples (Rosleff-Soerensen et al. 2012; Saqab & Bourget 2016), although
372 such features may be situated outside of the 3D seismic volume. Alternatively, the reefs
373 within the Farsund Basin may be located in a natural sheltered environment.

374 **5.4 Egersund and Tau formations – Deposition of anoxic shales**

375

376 The Sandnes Formation is overlain by the Upper Jurassic Egersund and Tau
377 Formations (Figure 3, 5). As determined from boreholes regionally, including well 11/5-1 in
378 the Farsund Basin, these formations typically comprise organic-rich shales (Figure 5). Within
379 the Farsund Basin, the Tau Formation has a slightly elevated Gamma Ray value (c. 120 API)
380 when compared to the underlying Egersund Formation (c. 110 API) (Figure 5). Both
381 formations are associated with a poorly reflective seismic facies within the basin (Figure 3,
382 5). Based on the observations outlined above, we interpret that the deposition of both the
383 Egersund and Tau formations occurred in a low-energy environment, with the presence of
384 pyritic and glauconitic horizons suggesting periodic anoxic conditions (Figure 5). Such an
385 environment may indicate a sea level rise and marine transgression since the deposition of the
386 Sandnes Formation, with deposition occurring in a deep marine environment, or may
387 alternatively indicate deposition within a restricted, low-energy shallow-water environment
388 (Van Der Zwaan & Jorissen 1991).

389 **5.5 Sauda Formation - Delta progradation**

390

391 A package of high-amplitude reflections is present at the top of the Jurassic interval,
392 corresponding to the Sauda Formation in well 11/5-1 (Figure 3, 11). This reflection package
393 is c. 40 ms TWT (c. 50 m) thick, thins southwards, and is associated with lateral changes in
394 amplitude and low-angle clinoform sequences that downlap towards the south (Figure 11).
395 These downlap terminations often correspond to the areas of amplitude brightening (Figure

396 11). The top and base of the high amplitude reflection package was mapped throughout the
397 3D volume, along with individual internal horizons. Seismic attributes were extracted from
398 between these top and base horizons (Figure 11).

399 RMS amplitude, spectral decomposition and dip azimuth seismic attributes highlight a
400 series of divergent, curvi-linear lineations in plan-view, defining high- and low-amplitude
401 packages of varying frequency (Figure 12). Each band is c. 400 m wide, diverges westwards
402 and displays a concave-to-south planform geometry. The bands are arranged into a series of
403 discordant sets and thus truncate each other, at either low (i.e. Sets 1-3 in Figure 12d) or high
404 angles (i.e. Set 4 in Figure 12d). Additional internal sets and truncations may tentatively be
405 present, although these are not clear and accurately delineated within the data (Figure 12).
406 The lineations are ubiquitous across the whole of the study area apart from across the
407 footwall of the present-day Fjerritslev South Fault, where the Sauda Formation is absent due
408 to erosion across the footwall of the fault (Figure 2, 12). The lineations are seemingly
409 unaffected by the Fjerritslev North Fault, which cross-cuts but does not noticeably offset the
410 lineations (Figure 12). Both the Fjerritslev North and Fjerritslev South Faults were not
411 present at this time, becoming active in post-Sauda times. A set of N-S striking lineations
412 (Set 4) are present to the northwest of the area and appear to correspond to the footwall of
413 NS1, which was inactive at this time (Set 4; Figure 12). These lineations are concave to the
414 east and diverge to the southwest. These N-S striking lineations also appear unaffected by the
415 Fjerritslev North Fault, although they align with and are located along the footwall of NS1,
416 suggesting this Triassic fault may have had some topographic expression at this time (Figure
417 12d). Faint lineations are identifiable in the southeast (Figure 12); these lineations are not
418 associated with the Sauda Formation, which thins northwest of the area, but instead are
419 related to subcrops of truncated underlying strata associated with salt mobilisation in this
420 area. In some instances there appear to be mutual cross-cutting relationships between

421 individual sets of lineations (i.e. Set 2 and Set 4 in Figure 12d), rather than truncations
422 against one another. However, these cross-cutting relationships are most likely due to signal
423 mixing within the attribute extraction window; i.e. closely superposed sets produce cross-
424 cutting relationships meaning their relative age cannot be distinguished in plan-view (Figure
425 12). The prominent lineations observed in plan-view (Figure 12) appear to correspond to the
426 downlap terminations of clinoform sequences, or where the clinoform sequences thin below
427 seismic resolution in cross-section (Figure 11).

428 Discordant sets of high-amplitude lineations identified in seismic reflection data,
429 superficially similar to those observed here, have previously been interpreted as ancient
430 shoreface beach ridge environments (Jackson et al. 2010; Klausen et al. 2015; Klausen et al.
431 2016). Such beach ridge systems typically comprise sand-rich ridges separated by elongate,
432 typically lower energy, depressions (Otvos 2000), and form cusped, concave-to-coastline
433 morphologies comprising multiple discordant sets, formed through longshore drift (Billy et
434 al. 2014; Vespremeanu-Stroe et al. 2016). Although geometrically similar, based on the lines
435 of evidence outlined below we discount a beach-ridge origin for the lineations within the
436 Farsund Basin. Firstly, the amplitude changes associated with the upper Jurassic curvi-linear
437 features within the Farsund Basin are located downdip, or below the small-scale clinoform
438 sequences (Figure 11), rather than being associated with the topsets as would be expected
439 with a beach ridge interpretation (e.g. Jackson et al. 2010; Billy et al. 2014). Instead, the
440 observed amplitude brightening may represent the tuned seismic response of the breakpoint
441 (Dreyer et al. 2005) or down-dip terminations of the clinoforms themselves (Eide et al. 2017).
442 Secondly, the concave-to-south planform geometries of the lineations would suggest that the
443 paleo-shoreline was north-facing, an interpretation largely incompatible with the regional
444 setting of the basin during the Late Jurassic, which was open to the south (Figure 1, 12). An
445 additional and final argument against a beach ridge origin for these lineations lies in their

446 regional context. Using regional 2D seismic data, the high-amplitude lineations can be traced
447 outside of the 3D volume. Here, they correspond to the lateral terminations of larger, lobate,
448 high-amplitude packages that thicken northwards (Figure 13, 14). Overall, these packages are
449 retrogradationally stacked, with clinoforms in younger packages downlapping onto the tops
450 of older, underlying clinoform packages (Figure 13), causing the overall thickness of the
451 Sauda Formation to increase northwards. This retrogradational stacking patterns suggests
452 deposition during a period of relative sea level rise, at a time when the rate of accommodation
453 generation outpaced sediment accumulation rates.

454 Individual clinoform-bearing packages are also partitioned laterally, forming a series
455 of discrete lobes that are identified via concordant lineations and terminal downlapping
456 reflections around their margins. The lateral terminations are also associated with an increase
457 in amplitude as the package thins below seismic resolution and, we suggest, constructively
458 tune (Figure 14). Based on these terminations we identify four main lobes, with the
459 easternmost margin of the eastern lobe defined by an area of amplitude brightening (Figure
460 14).

461 The lobes forms an arcuate geometry in plan-view (Figure 15). Individual lobes
462 prograde southwards, are c. 100 ms TWT (c. 140 m) thick and are 20-40 km wide (Figure 14,
463 15). They continue northwards into the Varnes Graben, which may represent a sediment
464 fairway from the mainland (Figure 13), although a lack of data coverage in this area means
465 their geometry cannot be constrained. As with the lineations identified in the 3D volume
466 (Figure 12), individual lobes identified on the 2D data display discordant relationships with
467 one another as younger lobes overlap and stack above and adjacent to older lobes (Figure 14,
468 15). The central lobe (Lobe 3) corresponds to the major lineations observed within the 3D
469 volume (Sets 1 and 2; Figure 12). This lobe is situated at shallower stratigraphic levels and
470 appears to overlap Lobe 2 situated to the east (Figure 15). Set 3 within the 3D volume may

471 also represent an older, stratigraphically deeper lobe (Lobe 1; Figure 15) that has been
472 covered by lineation sets 1 and 2 of Lobe 3 (Figure 12, 15). Lobe 3 appears to be overlain by
473 Lobe 4 to the west, which incorporates the lineations observed along the footwall of NS1 (Set
474 4, Figure 12d), as the thickness of the Upper Jurassic Sauda Formation increases westwards
475 (Figure 14). This thickness change is representative of increased lobe stacking to the north
476 and west (Figure 13, 15). We suggest that clinoform downlap terminations within individual
477 lobes may give rise to the lineation sets observed in the 3D data (Figure 12). Furthermore, the
478 overprinting and vertical stacking of different lobes may give rise to the discordant
479 truncations of the lineation sets observed in the 3D data (Figure 12), with older lobes being
480 partially overlapped by younger ones (Figure 15).

481 Based on this regional information, and in conjunction with the evidence outlined
482 previously, we interpret that the lineations within the Upper Jurassic Sauda Formation
483 correspond to the downlap termination of clinoforms within a series of deltaic lobes. The
484 lobes prograded into an unconfined basin setting, with lobe avulsion causing them to stack
485 laterally and vertically (Bridge & Leeder 1979; Jones & Schumm 1999). This interpretation is
486 based on: i) the lobate geometry of the individual sequences (Figure 14, 15); ii) lateral
487 downlap terminations at the margins of individual lobes (Figure 13, 15); iii) small-scale
488 clinoforms indicative of deposition within a relatively shallow-water environment (Patruno et
489 al. 2015a; Eide et al. 2017) (Figure 11, 13); iv) retrogradational stacking of individual lobes
490 indicating the generation of accommodation outpaced sediment accumulation rate, potentially
491 during a period of relative sea level rise (Figure 13); and v) progressive landward onlap of the
492 Sauda Formation by Lower Cretaceous strata (Figure 13, 14). The Sauda Formation overlies
493 the Egersund and Tau formations (Figure 5), which were deposited within an anoxic
494 environment. A corollary of the interpretation here is that these anoxic shales were likely
495 deposited within a shallow marine environment (Van Der Zwaan & Jorissen 1991), rather

496 than in deep-water, as the latter would require a drastic shallowing between the deposition of
497 the two formations.

498 **6 Discussion**

499

500 Our model for the geomorphological evolution of the Farsund Basin, and our
501 interpretations of the different facies types present (Figure 16), differs drastically from
502 regional tectono-stratigraphic models of the area (Figure 1b) (Johannessen & Andsbjerg
503 1993; Andsbjerg 2003; Mannie et al. 2014; Mannie et al. 2016). Here, we first compare and
504 contrast our model for the geomorphological evolution of the Farsund Basin outlined above
505 to that more regionally, before discussing the implications for the structural evolution of the
506 basin and regional tectonic activity, and the viability of petroleum systems in the area.

507 **6.1 Regional paleo-geographical setting**

508

509 The North Sea represented a predominately non-marine environment during the
510 Permian, as recorded by deposition of the Rotliegend Group (Glennie 1997; van Wees et al.
511 2000; Glennie et al. 2003). Deposition of Zechstein salt in the Upper Permian occurred
512 during a marine transgression and basin flooding (Glennie 1997; Glennie et al. 2003). East of
513 the Farsund Basin, Jackson & Lewis (2013) define the depositional limit of mobile Zechstein
514 salt striking ESE across the Lista Nose Fault Blocks (Figure 1). We find that this limit
515 continues eastwards along-strike across the southern margin of the Farsund Basin, and did not
516 extend north as far as previously described (Heeremans et al. 2004) (Figure 1). The local
517 occurrence of small-scale, likely fluvio-deltaic, clinoforms (Patruno et al. 2015a) (Figure 6),
518 and the non-marine Smith Bank and Skagerrak formations regionally (e.g. Goldsmith et al.
519 1995; McKie & Williams 2009; Jarsve et al. 2014), indicates a return to a sub-aerial
520 environment during the Triassic. The Triassic clinoforms were likely sourced from mainland

521 Scandinavia to the north, and likely prograded southwards through the Varnes Graben
522 (Figure 1).

523 Following Early-Mid Jurassic uplift, erosion and eventual deflation associated with
524 the Mid North Sea thermal dome (Underhill & Partington 1993), the first formation to be
525 preserved regionally was the Middle Jurassic Bryne Formation. This formation is
526 encountered in the Egersund Basin, Norwegian-Danish Basin and the Danish Central Graben,
527 where it consists of stacked fluvial and floodplain deposits deposited in a coastal-plain
528 environment (Sørensen et al. 1992; Johannessen & Andsbjerg 1993; Andsbjerg 2003;
529 Michelsen et al. 2003; Mannie et al. 2014; Mannie et al. 2016). Within the Farsund Basin, the
530 Bryne Formation is represented by two E-trending channels deposited within a fluvio-deltaic
531 environment (Figure 8e). At a regional scale the E-W orientation of these channels may be
532 influenced by the Mid Jurassic thermal dome (Underhill & Partington 1993), flowing away
533 from the site of maximum uplift. Alternatively, and in the authors view more likely, channel
534 orientation may be controlled by more local uplift related to the Lista Nose Fault Blocks and
535 Stavanger Platform to the west (Figure 1).

536 The Middle-Upper Jurassic (Callovia) Sandnes Formation documents a basinwide
537 marine transgression, transitioning from a sub-aerial to shallow marine depositional
538 environment, as observed elsewhere within the North Sea (Michelsen et al. 2003; Mannie et
539 al. 2014; Mannie et al. 2016). This transgression was driven by a eustatic sea-level rise (Vail
540 & Todd 1981; Sørensen et al. 1992), and may have been further augmented by rift-related
541 thermal subsidence relating to a Permian-Triassic rift phase (Ziegler 1992). Within the
542 Farsund Basin, the Sandnes Formation is manifest as a series of carbonate patch reefs (Figure
543 10), whereas elsewhere, including in the adjacent Egersund Basin, it contains only
544 siliciclastic sediments (Figure 1b, 16) (e.g. Sørensen et al. 1992; Mannie et al. 2014; Mannie
545 et al. 2016). The formation of carbonate patch reefs requires a lack of clastic sedimentation

546 within a relatively sediment starved basin. The lack of sediment within the Farsund Basin at
547 this time, compared to the Egersund Basin (Mannie et al. 2014; Mannie et al. 2016) may
548 reflect differences in their respective onshore source areas, and suggests that they were not
549 linked at this time.

550 In the Egersund Basin, facies shallow eastwards, from a fully marine environment to
551 a shoreface setting along the margin of the Stavanger Platform (Mannie et al. 2014). A
552 similar water depth change occurs within the Farsund Basin, although still largely within a
553 shallow-marine domain. Geomorphological features suggest relatively deeper water depths in
554 the east, represented by taller and, we infer, deeper-water patch reefs (Figure 9, 10, 16), and a
555 relatively shallow water depth towards the west which resulted in a dominance of shorter and
556 wider patch reefs. These complementary east- and west-facing shorefaces, and their
557 associated distinct facies belts (i.e. carbonate in the east and siliciclastic in the west) indicate
558 a relative high between the Egersund and Farsund Basins, potentially represented by
559 Stavanger Platform and Lista Nose Fault Blocks (Hamar et al. 1983; Sørensen et al. 1992).
560 One such topographic high, the Eigerøy Horst, continues northwards, as a series of
561 bathymetric highs termed the Hydra Mountains, to the Norwegian mainland where it may
562 reflect an onshore drainage divide (Rise et al. 2008).

563 Further relative sea-level increase is recorded by the deposition of the anoxic shales of
564 the Egersund and Tau formations (Vollset & Doré 1984; Sørensen et al. 1992). Cessation of
565 carbonate patch reef growth may have occurred due to a basin-wide transgression, or the
566 added input of the anoxic shales (Figure 16). Fine grained siltstones and claystones
567 comprising the Sauda Formation were deposited during the Upper Jurassic (Vollset & Doré
568 1984; Mannie et al. 2014), with a series of southwards-prograding and avulsing deltaic lobes
569 identified within the Farsund Basin (Figure 15, 16). This deltaic system has an extra-basinal
570 source, likely the Norwegian mainland, and was transported through the Carboniferous-

571 Permian-aged Varnes Graben, a sediment pathway during the Triassic (Heeremans et al.
572 2004; Jarsve et al. 2014). Lobe 4 however, may have a local sediment source, related to
573 degradation of the Eigerøy Horst, which in this area forms the footwall of the Farsund North
574 Fault (Figure 15). As with the stratigraphically older patch reefs, the deltaic lobes are also
575 restricted westwards of, and are not present on, the Stavanger Platform (Figure 17).

576 West of the Stavanger Platform, additional deltaic sequences, the Hardangerfjord and
577 Sognefjord units, are present within the Sauda Formation, sourced from and draining western
578 Norway (Dreyer et al. 2005; Somme et al. 2013; Patruno et al. 2015b) (Figure 17). Wells
579 penetrating the proximal part of the Hardangerfjord unit penetrate a mudstone dominated unit
580 (Somme et al. 2013), whereas the Sognefjord unit has been shown to be more sandstone
581 dominated (Patruno et al. 2015b). Within the Farsund Basin, well 11/5-1 penetrates a silty
582 sandstone/sandstone interval corresponding to the distal part of the delta sequence;
583 furthermore, the surrounding sediments are largely dominated by mudstones and siltstones
584 (Figure 5), so a more sandstone-rich interval would produce the observed large impedance
585 contrast (Figure 11, 13).

586 The partitioning between the Farsund deltaic sequence described here, and the
587 Hardangerfjord unit located west of the Stavanger Platform appear to reflect the location of
588 the drainage divide onshore Norway (Figure 17). Sediments sourced from west of the divide
589 are deposited into the Hardangerfjord unit (Somme et al. 2013), and those east of the divide
590 being deposited into the Farsund Basin and Skagerrak Sea (Somme et al. 2013; Jarsve et al.
591 2014) (Figure 17). The offshore continuation of this divide may be represented by the highs
592 of the Eigerøy Horst, Stavanger Platform and Lista Nose Fault Blocks (Hamar et al. 1983;
593 Skjerven et al. 1983) (Figure 17).

594 We have shown that the Farsund Basin contains different facies associations and
595 experienced a markedly different tectono-stratigraphic evolution to basins to the west,
596 separated by the Stavanger Platform and Lista Nose Fault Blocks. This may correspond to a
597 boundary between different structural domains, between Caledonian Orogeny and post-
598 orogenic collapse-dominated tectonics to the west (Phillips et al. 2016), and an evolution
599 dominated by the Sorgenfrei-Tornquist Zone and the Tornquist trend to the east (Mogensen
600 & Jensen 1994; Thybo 2000; Mogensen & Korstgård 2003; Phillips et al. 2018) (Figure 17).

601 **6.2 Implications for tectonic activity**

602

603 The Mesozoic structural evolution of this area is relatively understudied (Jensen &
604 Schmidt 1993; Phillips et al. 2018). Here we use inferences from our proposed
605 geomorphological evolution of the Farsund Basin to place additional constraints on its
606 tectono-stratigraphic evolution along with more regional tectonics.

607 The depositional limit of the Zechstein salt reflects relative structural highs present at
608 the time of deposition (Figure 1). Onlapping of the salt onto the southern margin of the
609 Farsund Basin indicates that, at that time, the area to the north formed part of the Stavanger
610 Platform, prior to later activity along the Fjerritslev North and South faults. This is in
611 agreement with structural observations that the Farsund Basin did not exist in its present form
612 until the Early Cretaceous (see Phillips et al. 2018). An abrupt step of c. 7 km is observed in
613 the limit across NS2 (Figure 1). This step may reflect pre-existing topography within the
614 basin at the time of deposition, post-depositional modification and translation of the boundary
615 due to later fault activity, or a combination of both. NS2, along with other N-S striking faults
616 may have been active during the Carboniferous-Permian extensional event (Heeremans &
617 Faleide 2004; Heeremans et al. 2004), although due to a lack of imaging at depth within our
618 seismic data, we are unable to confirm this. Pre-existing fault-related relief could cause such

619 a step in the depositional limit of mobile salt (Clark et al. 1998); similar steps are observed
620 along-strike relating to the Stavanger Fault system (Figure 1) (Jackson & Lewis 2013).
621 Additionally, the limit of the salt basin may have been modified post-deposition, perhaps
622 relating to Early Jurassic sinistral strike-slip activity (Phillips et al. 2018).

623 East-trending fluvial channels within the Bryne Formation were, at least in part,
624 controlled by the presence of thin-skinned, salt detached faults. A key observation is that
625 these E-trending channels are not influenced by the major E-W striking faults, in particular
626 the Fjerritslev South Fault, that delineate the present-day morphology of the basin. This
627 concurs with structural observations, i.e. the lack of syn-kinematic pre-Cretaceous strata
628 (Figure 3, 6), that the E-W faults were not active and had no surface expression at this time.
629 The widening of fluvial channels across NS2 occurs across a subtle topographic gradient,
630 interpreted as the paleo-shoreline. This topographic gradient may be related to differential
631 compaction of underlying Triassic strata across NS2.

632 East-trending structures also have negligible influence on the formation and
633 morphology of features within the Sandnes Formation. Patch reef morphology is unchanged
634 across the E-W striking Fjerritslev North and South Faults, indicating that they grew in
635 similarly shallow water depths (Figure 10) (Kendall & Schlager 1981). Conversely, patch
636 reef morphology changes markedly across N-S striking faults, from short, wide reefs on the
637 footwall, to tall, narrow reefs on the hangingwall (Figure 9, 10). Water depth has previously
638 been shown to be a key factor in determining carbonate facies and patch reef morphology,
639 with shallower water depths associated with shorter, wider reef morphologies (Brock et al.
640 2008), and favouring the formation of patch reefs over more continuous ridges (Colpaert et
641 al. 2007; Purkis et al. 2015). Thus, we infer this change in reef morphology represents a
642 change in water depth associated with the aforementioned topographic gradient across NS2
643 (Figure 9). Those patch reefs that grow in the slightly deeper water environment, i.e. the

644 hangingwall of NS2, exhibit catch-up growth as they attempt to reach shallower depths,
645 forming tall, narrow structures (Kendall & Schlager 1981; Schlager 1981; Saqab & Bourget
646 2016). On the other hand, the wider patch reefs situated at shallow water level, i.e. the
647 footwall of NS2, have no requirement for this catch-up growth and undergo keep-up growth,
648 preferentially growing laterally, forming shorter, wider structures (Brock et al. 2008; Saqab
649 & Bourget 2016). The occurrence of this catch-up/keep-up growth mechanism indicates that
650 the growth of these structures was sensitive to water depth, and therefore that they formed as
651 tropical carbonate reefs, as opposed to cool-water carbonates or carbonate mud mounds
652 (Schlager 2000). Late Jurassic ocean temperatures were relatively equilibrated across the
653 Tethyan Ocean, allowing tropical reefs to form across a large latitude range, including the
654 Farsund Basin (Leinfelder 1994).

655 Following the deposition of the Egersund and Tau formations, a series of southwards
656 prograding deltaic lobes were deposited in the Farsund Basin, forming part of the Upper
657 Jurassic Sauda Formation. Lobe geometry appears unaffected by any underlying relief, with
658 the Fjerritslev North and South faults now cross-cutting lobes. As they are now offset, this
659 implies that no fault-related topography was present at the time of deposition and that the
660 lobes were deposited in a relatively unconfined setting (Somme et al. 2013; Zhang et al.
661 2016). The lack of Upper Jurassic deltaic systems across the footwall of the Fjerritslev South
662 Fault may be due to erosion following post-depositional fault activity and sub-aerial exposure
663 of the footwall. Based on this, we infer that activity along the E-W Fjerritslev North and
664 South faults in the Farsund Basin began in the Early Cretaceous, following the deposition of
665 the deltaic system. Conversely, fault activity within the Egersund Basin started earlier, in the
666 latest Jurassic, affecting the thickness and distribution of different facies (Mannie et al. 2014;
667 Mannie et al. 2016). In the Farsund Basin, this likely corresponds to the same extensional
668 event, with the age of the deltaic system straddling the Jurassic/Cretaceous boundary.

669 The Sauda Formation represents an input of sandstone deposited during an overall net
670 marine transgression (Mannie et al. 2016). This input of clastic material, both in the Farsund
671 Basin and offshore west Norway (Somme et al. 2013), corresponded to the late pre-rift to
672 peak-syn-rift stage of Late Jurassic-Early Cretaceous extension (Brun & Tron 1993; Bell et
673 al. 2014). The Early Cretaceous succession within the Farsund Basin predominately consists
674 of relatively deep marine sediments. Deposition of these sediments was associated with a
675 deepening of the Farsund Basin relating to Early Cretaceous tectonic activity (Mogensen &
676 Jensen 1994). This likely represents the same regional rift event documented to the west,
677 responsible for the deposition of the Hardangerfjord Delta sequence, although this event may
678 be regionally diachronous (Somme et al. 2013; Mannie et al. 2016).

679 **6.3 Implications for petroleum systems development of the Farsund Basin**

680

681 In constraining the geomorphological evolution of the Farsund Basin, we have also
682 identified a series of potential carbonate and clastic reservoirs that may form part of viable
683 petroleum systems. Channels identified within the Bryne Formation (Figure 7) are likely
684 composed of fluvial sandstones (Ryseth et al. 1998). In addition, carbonates, including patch
685 reefs such as those identified within the Sandnes Formation (Figure 9, 10), and offshore
686 deltaic systems akin to those within the Sauda Formation (Figure 11, 12, 15) have previously
687 been shown to represent viable petroleum reservoirs (Montgomery 1996; Moore 2001; Saller
688 et al. 2008).

689 The reservoir potential of the Sandnes Formation patch reefs is complicated due to
690 distinguishing between primary and secondary porosity within the reefs themselves (Enos &
691 Sawatsky 1981). Original porosity within carbonates can be enhanced through dissolution of
692 the host material, or alternatively, may be destroyed and infilled by secondary cementation.
693 This secondary porosity is dependent on a number of different factors. Typically, patch reefs

694 consist of a cemented core containing negligible porosity, with a less cemented, more porous
695 surrounding framework (Enos & Sawatsky 1981). The high amplitude core and lower
696 amplitude rim of the carbonate patch reefs as imaged in seismic data (Figure 9, 10a) may
697 potentially reflect such a change in the degree of cementation, from a relatively compacted
698 and cemented core, to a more porous rim. These complications notwithstanding, working
699 patch reef plays have been discovered, such as the Lime Valley Pinnacle Reef Play, in Texas,
700 USA (e.g. Montgomery 1996).

701 Stratigraphic and structural traps and seals are present within the Farsund Basin. The
702 Zechstein salt would act as a regional seal throughout large parts of the area. However, areas
703 to the north of the depositional limit of the salt may allow vertical migration into the Jurassic
704 section (Figure 1). The carbonate patch reefs and fluvial channel systems are largely overlain
705 by and encased in shales of the Egersund and Tau formations (Figure 3, 5). In addition, the
706 isolated nature of the fluvial systems and the patch reefs allow them to represent discrete
707 volumes. The lateral terminations of the Upper Jurassic deltaic lobes would also be expected
708 to have stratigraphic traps at their margins and are sealed by overlying Lower Cretaceous
709 claystones and siltstones. Variable reservoir may be expected within the deltaic lobes; sandier
710 material would be expected in the topsets and foresets of the clinofolds compared to the
711 bottomsets, with a potential reduction in reservoir quality also expected around the distal
712 margins of the lobes (Patruno et al. 2015a; Patruno et al. 2015b). Due to the main period of
713 faulting along the E-W faults occurring following the deposition of the Jurassic interval,
714 including these potential reservoir units (Figure 3, 6), a number of structural traps may also
715 be present. Early Cretaceous faulting offsets and partitions the Upper Jurassic deltaic system
716 into a series of discrete potential reservoir units (Figure 16).

717 In addition to these reservoirs, a number of potential source rocks are present
718 throughout the area, each of varying maturity and likelihood of viability. The organic-rich

719 shales of the Tau Formation may be oil-mature in the centre of the Farsund Basin (Skjerven
720 et al. 1983; Sørensen & Tangen 1995; Petersen et al. 2008). These correspond regionally to
721 the Kimmeridge Clay and Draupne shales in the UK and Norwegian North Sea, respectively,
722 which represent key source rock intervals in each area. The Tau Formation shales may be
723 able to act as a local source rock for the identified Jurassic reservoirs. Regionally, the
724 Cambrian aged Alum shales, situated to the east of the area (Petersen et al. 2008), may be
725 mature and could act as a potential source rock in this region, although potential migration
726 pathways into the Jurassic interval in this area seem far-fetched. Through constraining its
727 geomorphological evolution we have identified and mapped key components of the
728 petroleum system within the Farsund Basin, and have shown how seismic attribute driven
729 interpretation can aid the imaging and mapping of petroleum systems in frontier areas.

730 **7 Conclusions**

731

732 In this study we have used a seismic attribute-driven approach to determine the
733 geomorphological evolution of the Triassic-Jurassic succession in the Farsund Basin,
734 offshore south Norway. Having established this local evolution, we link this to the tectono-
735 stratigraphic evolution of the wider area and assess the viability of any potential petroleum
736 systems. Overall, we find that:

- 737 1. The depositional limit of mobile Zechstein salt trends E-W across the southern margin
738 of the Farsund Basin, onlapping the edge of the Stavanger Platform at the time of its
739 deposition. A step in the depositional limit likely reflects base-salt relief relating to a
740 pre-existing fault scarp, but may also be a result of post-depositional modification of
741 the basin.
- 742 2. The geomorphological evolution of the Farsund Basin reflects an overall marine
743 transgression, documented through the identification of fluvial river systems of the

744 Middle Jurassic Bryne Formation, shallow marine patch reefs developed within the
745 Sandnes Formation, and Late Jurassic delta lobes within the Sauda Formation.

746 3. The morphology of the identified geomorphological features offer insights into the
747 paleo-geographical setting of the basin. Paleo-topography, formed as a result of
748 differential compaction across previously active faults, represents the paleo-shoreline
749 and reflects a change in water depth throughout the deposition of the Bryne and
750 Sandnes formations. The Upper Jurassic deltaic systems are unaffected by, and were
751 therefore deposited prior to, the onset of faulting within the Farsund Basin

752 4. The tectono-stratigraphic evolution of the Farsund Basin differs markedly to that of
753 the Egersund Basin to the west, due to the presence of a partition between the two
754 areas. This partition is formed of structural highs corresponding to the Stavanger
755 Platform and Lista Nose Fault Blocks offshore, and potentially the drainage divide
756 onshore. These differing tectono-stratigraphic evolutions between the two areas
757 reflects a difference in their regional tectonic settings, the evolution of the Egersund
758 Basin area is controlled by Caledonian orogeny and orogenic collapse related
759 structures, and the Farsund Basin by the underlying Sorgenfrei-Tornquist Zone.

760 5. Through this seismic geomorphological analysis we have identified a series of
761 potential reservoirs, including fluvial systems, carbonate patch reefs, and offshore
762 deltaic lobes, which along with seals and local sources within the Tau Formation, may
763 form parts of working petroleum systems within the area.

764 This study showcases how seismic attributes and seismic geomorphological analysis can
765 be used to determine the tectono-stratigraphic evolution of rift basins. These techniques are
766 able to identify potential petroleum systems, representing a vital tool for the exploration of
767 relatively underexplored frontier basins, and also offer insights into the structural evolution
768 and wider tectonic settings of relatively underexplored basins.

769 **Acknowledgements**

770

771 This contribution forms part of the MultiRift project, funded by the Research Council of
772 Norway's PETROMAKS programme (project number 215591) and Statoil to the University
773 of Bergen and partners Imperial College, University of Manchester and University of Oslo.
774 We thank the editor, Philip Ringrose, along with Bonita Barrett-Crosdil and an anonymous
775 reviewer for their detailed reviews that greatly improved the quality of the manuscript. We
776 also would like to thank PGS for allowing us to show and use the seismic data presented in
777 this study and GeoTeric for providing us with academic licences for the software to undertake
778 the spectral decomposition in the project. We would also like to thank Schlumberger for
779 providing academic licences of the Petrel software to Imperial College.

780

781 **Appendix A – Seismic attributes**

782 Seismic attribute analysis was used to gain more information about the facies present across different
783 stratigraphic levels within the Farsund Basin. RMS amplitude, variance, amplitude contrast, and
784 spectral decomposition were calculated along a series of key stratigraphic horizons, with the attributes
785 calculated across a window bounding the interval of interest specified in the text.

786 *Root mean squared (RMS) amplitude* is a measure of the absolute strength of the reflection,
787 regardless of its polarity; stronger, brighter reflections are represented by higher RMS amplitude
788 values.

789 *Variance* represents a measure of discordance between individual traces within the seismic data. The
790 larger the difference between adjacent traces, the higher the variance value; therefore, this seismic
791 attribute typically highlights the edges of discrete structures.

792 *Amplitude contrast* works in a similar way to the variance attribute, quantifying the lateral contrast in
793 amplitude between adjacent traces.

794 ***Dip azimuth*** quantifies the dip magnitude and dip direction of the reflections, with the azimuth
795 represented by a colour within a spectrum, and the dip by the shade of the colour. This attribute is
796 calculated for each voxel within the data.

797

798 In addition to amplitude-derived attributes, we also investigated a number of frequency-derived
799 attributes, to further interrogate the seismic reflection data. The frequency of the data with depth is
800 shown in Figure 4, with an average frequency within the Jurassic interval of c. 35 Hz. Frequency is
801 inherently linked to unit thickness, higher frequency values are able to resolve thinner units (Slatt
802 2006; Brown 2011).

803 ***Dominant frequency*** is a measure of frequency that accounts for both the instantaneous bandwidth
804 and frequency, representing a relatively smoothed frequency value.

805 ***Spectral decomposition*** represents a colour blend of discrete frequency values extracted from the
806 frequency spectrum of the data. The frequency spectrum of the data (Figure 4) is partitioned into a
807 series of bins (each 20 Hz wide) which correspond to a range of frequencies. We then assign three of
808 these frequency values to red, green and blue, representing low, medium and high frequency values,
809 respectively; the brightness of each colour represents the power that frequency component
810 contributes, i.e. red colours indicate a preponderance of lower frequencies, whereas structures with a
811 response from all three frequency windows are represented by white. In this study, we assign
812 frequency values of 22, 30 and 45 Hz to red, green and blue colours to produce our RGB spectral
813 decomposition colour blend.

814

815

816 **Figure captions**

817 **Figure 1** - A) TWT structure map showing the acoustic basement (Base upper Permian/Zechstein
818 salt) surface throughout the study area. Red circles represent wells throughout the area, note the high
819 density of well coverage in the Egersund Basin compared to the Farsund Basin. Also shown are the
820 location of the 3D seismic survey referred to in this study and the salt depositional limits proposed by
821 Jackson and Lewis (2013), Heeremans et al. (2014) and this study. B) Jurassic stratigraphic column.
822 Lithostratigraphy from Mannie et al. (2016), focused on well data from the Egersund Basin, is
823 contrasted against seismic data around well 11/5-1, located within the Farsund Basin. Note the lack of
824 Triassic and Middle-Lower Jurassic strata in well 11/5-1.

825 **Figure 2** – TWT structure maps of key stratigraphic horizons within the 3D volume located over the
826 southern margin of the Farsund Basin. See Figure 1a for location and Figure 1b for the stratigraphic
827 ages of horizons. A) TWT structure map of the Top Jurassic surface, dominated by the E-W striking
828 Fjerritslev North and Fjerritslev South Faults. Also present is the N-S striking NS2 fault. B) TWT
829 structure map of the stratigraphically deeper Base Jurassic Unconformity. C) TWT structure map of
830 the base Zechstein salt acoustic basement surface. This surface is dominated by a series of N-S and E-
831 W striking faults.

832 **Figure 3** – Uninterpreted and interpreted seismic sections across the study area showing the Triassic
833 and Jurassic intervals. Note that the Jurassic interval appears restorable across the Fjerritslev South
834 Fault, indicating that fault activity occurred later, during the Early Cretaceous. Also, the upper
835 Jurassic interval appears eroded from the footwall of the Fjerritslev South Fault. Structures analysed
836 in sections 5.1, 5.2, 5.3 and 5.5 are labelled on the interpreted section. See Figure 2 for location.

837 **Figure 4** – A) Frequency vs depth throughout the Farsund Basin in the vicinity of the 11/5-1 well.
838 Inset - closeup of the changing frequency with depth within the Jurassic interval. Frequency was
839 calculated within a 3-point moving average. Vertical resolution was also calculated at various depths.
840 B) Frequency spectrum for the 3D seismic volume. Also shown are the extracted frequency bins
841 combined to create the spectral decomposition seismic attribute.

842 **Figure 5** – Well log information and synthetic seismic for the Jurassic interval of well 11/5-1.
843 Synthetic seismic section was created using the RHOB and DT wireline logs of the well. A lack of
844 density data at around 1130-1180m results in a major discrepancy between the original and synthetic
845 seismic data. Otherwise, the synthetic provides a good match to the original seismic at the Rotliegend
846 Group and Sandnes Formation intervals, as well as the Sauda Formation.

847 **Figure 6** – Uninterpreted and interpreted seismic section showing the northwards limit of thin-
848 skinned, salt-detached faulting marking the northern depositional limit of mobile salt. Also note that
849 an undeformed clinof orm interval progrades southwards before being offset by thin-skinned faulting
850 to the south. See Figure 2 for location.

851 **Figure 7** – Uninterpreted and interpreted N-trending seismic sections across the southern margin of
852 the Farsund Basin, see Figure 2 for location. Two distinct high-amplitude features can be observed at
853 the base of the Jurassic interval corresponding to channel systems. Note that the channel systems are
854 predominately situated within the hangingwalls of the thin-skinned, salt-detached faults.

855 **Figure 8** – Seismic attribute maps of the southern margin of the Farsund Basin, calculated in a 25 ms
856 TWT window below the top of the high amplitude structures. A) TWT structure map of the area,
857 located at the intersection of the NS2 and Fjerritslev South faults. B) RMS amplitude seismic
858 attribute, highlighting two high amplitude E-trending channel-like features, widening across NS2. C)
859 Variance seismic attribute, further delineating the margins of the structures. D) Dominant frequency
860 attribute, showing the overall geometry of the features and showing a decrease in frequency in the
861 centre of the structure towards the east. E) Interpretation, based on the seismic attributes above, of
862 these features as a fluvial channel system, widening into a more deltaic environment across NS2.

863 **Figure 9** – Uninterpreted and interpreted seismic section showing a series of discrete high amplitude
864 structures within the Sandnes Formation. A wider, shorter structure is present on the footwall of NS2,
865 with taller, narrower structures on the hangingwall. See Figure 2 for location.

866 **Figure 10** – Compilation of seismic attributes extracted from a 50 ms TWT window above the Base
867 Jurassic Unconformity across the whole of the 3D seismic volume, see Figure 1 for location. A) RMS

868 amplitude highlighting high amplitude, sub-circular structures. B) Spectral decomposition,
869 highlighting sub-circular structures, including those on the hangingwall of NS2. C) Variance, showing
870 that the structures contain few internal discontinuities. D) Interpretation of the area, showing wider
871 sub-circular structures, interpreted as carbonate patch reefs, on the footwall of NS2 and smaller
872 structures on the hangingwall. E) Seismic section showing a composite reef, formed through the radial
873 growth and coalescence of two individual reefs. See Figure 10d for location. F) Seismic section
874 showing a reef offset by later faulting, implying a brittle nature. See Figure 10d for location.

875 **Figure 11** – Uninterpreted and interpreted seismic section showing lateral amplitude changes within
876 the upper Jurassic Sauda Formation. Two distinct sets can be identified (Set 2 and Set 3), defined by
877 downlap terminations of clinoform structures. Grey arrow corresponds to the location marked by the
878 grey arrow on Figure 12. See Figures 2 and 12 for location.

879 **Figure 12** – Seismic attribute maps across the 3D seismic volume extracted from a window between
880 the top and the base of the high amplitude package (see Figure 11). The white line indicates the
881 location of Figure 11, whilst the grey arrow corresponds to that shown on Figure 11. A) RMS
882 amplitude attribute map showing a series of concave to the south, curvilinear high amplitude
883 lineations. B) Spectral decomposition seismic attribute, highlighting internal lineation geometries and
884 relationships between individual sets. C) Dip azimuth of the lineations, further highlighting the
885 curvilinear and discordant nature of the lineation sets. D) Interpretation of the lineation sets. The
886 curvilinear lineations are arranged into a series of discordant sets that truncate each other at low
887 angles. A further, concave-to-the-east lineation set is present along the footwall of NS1. Note that the
888 lineations are not present across the footwall of the Fjerritslev South Fault and do not appear to be
889 influenced by the Fjerritslev North Fault.

890 **Figure 13** – Uninterpreted and interpreted N-S oriented regional 2D seismic section across the
891 Farsund Basin. See Figure 1 for location. The area also imaged in the 3D volume is situated to the
892 south. A series of deltaic systems are identified prograding southwards and aggrading and stacking
893 atop one another, as evidenced by downlap terminations. The base of the Sauda Formation is marked
894 as a reference horizon by a blue dashed line on the uninterpreted section.

895 **Figure 14** – Uninterpreted and interpreted E-W oriented regional 2D seismic section. See Figure 1 for
896 location. Three discrete deltaic lobes can be identified across the area, with lateral downlap
897 terminations observed either side. These lobes appear to thicken towards the west. The base of the
898 Sauda Formation is marked as a reference horizon by a blue dashed line on the uninterpreted section.

899 **Figure 15** – Compilation and map-view geometry of individual lobes associated with the fan system
900 in the Sauda Formation. The location of the 3D volume is shown by the black polygon whilst grey
901 lines mark the major faults. Individual lineation sets as identified in Figure 12 are labelled in blue.
902 Different structural elements are shown in various shades of grey. Fan geometries are based on lateral
903 downlap terminations within the 2D data (see Figure 13 and 14), and the lineations identified within
904 the 3D volume. A series of deltaic lobes are identified, prograding from the north and stacking
905 progressively towards the west.

906 **Figure 16** –Left. A) Coastal plain-shallow marine environment during the deposition of the Bryne
907 Formation with eastwards flowing fluvial systems widening into a more deltaic environment across
908 NS2. B) Patch reef development within a sheltered shallow marine environment during the deposition
909 of the Sandnes Formation. Wide, short patch reefs present in shallower water pass eastwards into a
910 deeper environment, consisting of tall, narrow patch reefs, across the NS2 fault. C) Progradation of
911 shallow marine deltaic systems from the north during the Late Jurassic and the deposition of the
912 Sauda Formation. Right – Tectono-stratigraphic chart showing the local evolution of the Farsund
913 Basin as evidenced in this study. N-S striking faults, NS1 and NS2, were active during the Triassic,
914 whereas E-W striking faults, i.e. the Fjerritslev North and South Faults, and the Farsund North Fault,
915 were active during Early Cretaceous rifting.

916 **Figure 17** – Regional tectono-stratigraphic setting of the study area during the Late Jurassic and
917 deposition of the Sauda Formation. The Farsund Basin is dominated by the progradation of the
918 Farsund Delta, whereas the Egersund Basin is dominated by the Hardangerfjord Delta, with the two
919 areas separated by the intervening structural high of the Stavanger Platform and Lista Nose Fault
920 Blocks.

921

922 **References**

923 Agirrezabala, L.M., Kiel, S., Blumenberg, M., Schäfer, N. & Reitner, J. 2013. Outcrop analogues of
924 pockmarks and associated methane-seep carbonates: A case study from the Lower Cretaceous
925 (Albian) of the Basque-Cantabrian Basin, western Pyrenees. *Palaeogeography, Palaeoclimatology,*
926 *Palaeoecology*, **390**, 94-115, <http://doi.org/http://dx.doi.org/10.1016/j.palaeo.2012.11.020>.

927

928 Andresen, K.J., Huuse, M., Schodt, N.H., Clausen, L.F. & Seidler, L. 2011. Hydrocarbon plumbing
929 systems of salt minibasins offshore Angola revealed by three-dimensional seismic analysis. *AAPG*
930 *Bulletin*, **95**, 1039-1065.

931

932 Andsbjerg, J. 2003. Sedimentology and sequence stratigraphy of the Bryne and Lulu formations,
933 middle Jurassic, northern Danish Central Graben. *The Jurassic of Denmark and Greenland.*
934 *Geological Survey of Denmark and Greenland Bulletin*, **1**, 301-347.

935

936 Bell, R.E., Jackson, C.A.L., Whipp, P.S. & Clements, B. 2014. Strain migration during multiphase
937 extension: Observations from the northern North Sea. *Tectonics*, **33**, 1936-1963,
938 <http://doi.org/10.1002/2014TC003551>.

939

940 Billy, J., Robin, N., Hein, C.J., Certain, R. & FitzGerald, D.M. 2014. Internal architecture of mixed
941 sand-and-gravel beach ridges: Miquelon-Langlade Barrier, NW Atlantic. *Marine Geology*, **357**, 53-
942 71, <http://doi.org/http://dx.doi.org/10.1016/j.margeo.2014.07.011>.

943

944 Bridge, J.S. & Leeder, M.R. 1979. A simulation model of alluvial stratigraphy. *Sedimentology*, **26**,
945 617-644, <http://doi.org/doi:10.1111/j.1365-3091.1979.tb00935.x>.

946

947 Brock, J.C., Palaseanu-Lovejoy, M., Wright, C.W. & Nayegandhi, A. 2008. Patch-reef morphology as
948 a proxy for Holocene sea-level variability, Northern Florida Keys, USA. *Coral Reefs*, **27**, 555-568.

949

950 Brown, A.R. 2011. *Interpretation of three-dimensional seismic data*. Society of Exploration
951 Geophysicists and American Association of Petroleum Geologists.

952

953 Brun, J.-P. & Tron, V. 1993. Development of the North Viking Graben: inferences from laboratory
954 modelling. *Sedimentary Geology*, **86**, 31-51.

955

956 Cartwright, J. & Huuse, M. 2005. 3D seismic technology: the geological 'Hubble'. *Basin Research*,
957 **17**, 1-20, <http://doi.org/10.1111/j.1365-2117.2005.00252.x>.

958

959 Chopra, S. & Marfurt, K.J. 2008. Emerging and future trends in seismic attributes. *The Leading Edge*,
960 **27**, 298-318, <http://doi.org/10.1190/1.2896620>.

961

962 Christensen, J.E. & Korstgård, J.A. 1994. The Fjerritslev Fault offshore Denmark - salt and fault
963 interactions. *First Break*, **12**, 31-42, <http://doi.org/10.3997/1365-2397.1994003>

964

965 Clark, J.A., Stewart, S.A. & Cartwright, J.A. 1998. Evolution of the NW margin of the North Permian
966 Basin, UK North Sea. *Journal of the Geological Society*, **155**, 663-676, <http://doi.org/DOI>
967 10.1144/gsjgs.155.4.0663.

968
969 Colpaert, A., Pickard, N., Mienert, J., Henriksen, L.B., Rafaelsen, B. & Andreassen, K. 2007. 3D
970 seismic analysis of an Upper Palaeozoic carbonate succession of the Eastern Finnmark Platform area,
971 Norwegian Barents Sea. *Sedimentary Geology*, **197**, 79-98,
972 <http://doi.org/http://dx.doi.org/10.1016/j.sedgeo.2006.09.001>.

973
974 Coward, M.P., Dewey, J.F., Hempton, M. & Holroyd, J. 2003. Tectonic evolution. *In*: Evans, D.,
975 Graham, C., Armour, A. & Bathurst, P. (eds) *The Millenium Atlas: petroleum geology of the central*
976 *and northern North Sea*, Geological Society of London.

977
978 Davies, R.J. & Stewart, S.A. 2005. Emplacement of giant mud volcanoes in the South Caspian Basin:
979 3D seismic reflection imaging of their root zones. *Journal of the Geological Society*, **162**, 1-4,
980 <http://doi.org/10.1144/0016-764904-082>.

981
982 Dreyer, T., Whitaker, M., Dexter, J., Flesche, H. & Larsen, E. 2005. From spit system to tide-
983 dominated delta: integrated reservoir model of the Upper Jurassic Sognefjord Formation on the Troll
984 West Field. *Geological Society, London, Petroleum Geology Conference series*, **6**, 423-448,
985 <http://doi.org/10.1144/0060423>.

986
987 Eide, C.H., Klausen, T.G., Katkov, D., Suslova, A.A. & Helland-Hansen, W. 2017. Linking an Early
988 Triassic delta to antecedent topography: Source-to-sink study of the southwestern Barents Sea margin.
989 *GSA Bulletin*, **130**, 263-283, <http://doi.org/10.1130/b31639.1>.

990
991 Enos, P. & Sawatsky, L.H. 1981. Pore networks in Holocene carbonate sediments. *Journal of*
992 *Sedimentary Research*, **51**, 961-985, <http://doi.org/10.1306/212f7df1-2b24-11d7-8648000102c1865d>.

993
994 Færseth, R.B. 1996. Interaction of Permo-Triassic and Jurassic extensional fault-blocks during the
995 development of the northern North Sea. *Journal of the Geological Society*, **153**, 931-944,
996 <http://doi.org/10.1144/gsjgs.153.6.0931>.

997
998 Fichler, C., Henriksen, S., Rueslaatten, H. & Hovland, M. 2005. North Sea Quaternary morphology
999 from seismic and magnetic data: indications for gas hydrates during glaciation. *Petroleum Geoscience*,
1000 **11**, 331-337, <http://doi.org/10.1144/1354-079304-635>.

1001
1002 Glennie, K.W. 1997. Recent advances in understanding the southern North Sea Basin: a summary.
1003 *Geological Society, London, Special Publications*, **123**, 17-29,
1004 <http://doi.org/10.1144/gsl.sp.1997.123.01.03>.

1005
1006 Glennie, K.W., Higham, J. & Stemmerik, L. 2003. Permian. *In*: Evans, D. (ed) *The Millenium Atlas:*
1007 *Petroleum geology of the Central and Northern North Sea*. The Geological Society of London.

1008
1009 Goldsmith, P.J., Rich, B. & Standring, J. 1995. Triassic correlation and stratigraphy in the South
1010 Central Graben, UK North Sea. *Geological Society, London, Special Publications*, **91**, 123-143,
1011 <http://doi.org/10.1144/gsl.sp.1995.091.01.07>.

1012
1013 Hamar, G., Fjaeran, T. & Hesjedal, A. 1983. Jurassic stratigraphy and tectonics of the south-
1014 southeastern Norwegian offshore. *Petroleum Geology of the Southeastern North Sea and the Adjacent*
1015 *Onshore Areas*. Springer, 103-114.

1016
1017 Heeremans, M. & Faleide, J.I. 2004. Late Carboniferous-Permian tectonics and magmatic activity in
1018 the Skagerrak, Kattegat and the North Sea. *Geological Society, London, Special Publications*, **223**,
1019 157-176.

1020
1021 Heeremans, M., Faleide, J.I. & Larsen, B.T. 2004. Late Carboniferous -Permian of NW Europe: an
1022 introduction to a new regional map. *Geol Soc London, Special Publication*, **223**, 75-88.

1023
1024 Holgate, N.E., Jackson, C.A.L., Hampson, G.J. & Dreyer, T. 2013. Sedimentology and sequence
1025 stratigraphy of the Middle–Upper Jurassic Krossfjord and Fensfjord formations, Troll Field, northern
1026 North Sea. *Petroleum Geoscience*, **19**, 237.

1027
1028 Holgate, N.E., Hampson, G.J., Jackson, C.A.-L. & Petersen, S.A. 2014. Constraining uncertainty in
1029 interpretation of seismically imaged clinofolds in deltaic reservoirs, Troll field, Norwegian North
1030 Sea: Insights from forward seismic models of outcrop analogs. *AAPG Bulletin*, **98**, 2629-2663.

1031
1032 Hovland, M., Talbot, M.R., Qvale, H., Olaussen, S. & Aasberg, L. 1987. Methane-Related Carbonate
1033 Cements in Pockmarks of the North-Sea. *Journal of Sedimentary Research*, **57**, 881-892.

1034
1035 Jackson, C.A.L. & Lewis, M.M. 2013. Physiography of the NE margin of the Permian Salt Basin:
1036 new insights from 3D seismic reflection data. *Journal of the Geological Society*, **170**, 857-860,
1037 <http://doi.org/10.1144/jgs2013-026>.

1038
1039 Jackson, C.A.L., Chua, S.T., Bell, R.E. & Magee, C. 2013. Structural style and early stage growth of
1040 inversion structures: 3D seismic insights from the Egersund Basin, offshore Norway. *Journal of*
1041 *Structural Geology*, **46**, 167-185, <http://doi.org/http://dx.doi.org/10.1016/j.jsg.2012.09.005>.

1042
1043 Jackson, C.A.L., Grunhagen, H., Howell, J.A., Larsen, A.L., Andersson, A., Boen, F. & Groth, A.
1044 2010. 3D seismic imaging of lower delta-plain beach ridges: lower Brent Group, northern North Sea.
1045 *Journal of the Geological Society*, **167**, 1225-1236.

1046
1047 Jackson, M.P.A. & Talbot, C.J. 1986. External Shapes, Strain Rates, and Dynamics of Salt Structures.
1048 *Geological Society of America Bulletin*, **97**, 305-323, <http://doi.org/Doi> 10.1130/0016-
1049 7606(1986)97<305:Essrad>2.0.Co;2.

1050
1051 Jarsve, E.M., Maast, T.E., Gabrielsen, R.H., Faleide, J.I., Nystuen, J.P. & Sasier, C. 2014. Seismic
1052 stratigraphic subdivision of the Triassic succession in the Central North Sea; integrating seismic
1053 reflection and well data. *Journal of the Geological Society*, **171**, 353-374,
1054 <http://doi.org/10.1144/jgs2013-056>.

1055
1056 Jensen, L.N. & Schmidt, B.J. 1993. Neogene uplift and erosion offshore south Norway: magnitude
1057 and consequences for hydrocarbon exploration in the Farsund Basin. *In: Spencer, A.M. (ed.) Spec.*
1058 *Publ. European Association of Petroleum Geoscientists*. Springer.

1059
1060 Johannessen, P.N. & Andsbjerg, J. 1993. Middle to Late Jurassic basin evolution and sandstone
1061 reservoir distribution in the Danish Central Trough. *Geological Society, London, Petroleum Geology*
1062 *Conference 				series*, **4**, 271-283, <http://doi.org/10.1144/0040271>.

1063
1064 Jones, L. & Schumm, S. 1999. Causes of avulsion: an overview *Fluvial sedimentology VI*. Spec. Publ.
1065 Int. Assoc. Sedimentol, **28**, 171-178.

1066
1067 Kallweit, R.S. & Wood, L.C. 1982. The limits of resolution of zero-phase wavelets. *GEOPHYSICS*,
1068 **47**, 1035-1046, <http://doi.org/10.1190/1.1441367>.

1069
1070 Kendall, C.G.S.C. & Schlager, W. 1981. Carbonates and relative changes in sea level. *Marine*
1071 *Geology*, **44**, 181-212.

1072
1073 Klausen, T.G., Ryseth, A., Helland-Hansen, W. & Gjelberg, H.K. 2016. Progradational and
1074 backstepping shoreface deposits in the Ladinian to Early Norian Snadd Formation of the Barents Sea.
1075 *Sedimentology*, **63**, 893-916, <http://doi.org/10.1111/sed.12242>.

1076
1077 Klausen, T.G., Ryseth, A.E., Helland-Hansen, W., Gawthorpe, R. & Laursen, I. 2015. Regional
1078 development and sequence stratigraphy of the Middle to Late Triassic Snadd Formation, Norwegian
1079 Barents Sea. *Marine and Petroleum Geology*, **62**, 102-122,
1080 <http://doi.org/http://dx.doi.org/10.1016/j.marpetgeo.2015.02.004>.

1081
1082 Kluesner, J.W., Silver, E.A., Bangs, N.L., McIntosh, K.D., Gibson, J., Orange, D., Ranero, C.R. &
1083 von Huene, R. 2013. High density of structurally controlled, shallow to deep water fluid seep
1084 indicators imaged offshore Costa Rica. *Geochemistry, Geophysics, Geosystems*, **14**, 519-539,
1085 <http://doi.org/10.1002/ggge.20058>.

1086
1087 Legler, B., Hampson, G.J., Jackson, C.A., Johnson, H.D., Massart, B.Y., Sarginson, M. & Ravnås, R.
1088 2014. Facies relationships and stratigraphic architecture of distal, mixed tide-and wave-influenced
1089 deltaic deposits: Lower Segó sandstone, western Colorado, USA. *Journal of Sedimentary Research*,
1090 **84**, 605-625.

1091
1092 Leinfelder, R.R. 1994. Distribution of Jurassic reef types: a mirror of structural and environmental
1093 changes during breakup of Pangea *Pangea: Global Environments and Resources*. CSPG Special
1094 Publications, AAPG Memoir, **17**, 677-700.

1095
1096 Lewis, M.M., Jackson, C.A.L. & Gawthorpe, R.L. 2013. Salt-influenced normal fault growth and
1097 forced folding: The Stavanger Fault System, North Sea. *Journal of Structural Geology*, **54**, 156-173,
1098 <http://doi.org/10.1016/j.jsg.2013.07.015>.

1099
1100 Magee, C., Duffy, O.B., Purnell, K., Bell, R.E., Jackson, C.A.L. & Reeve, M.T. 2016. Fault-
1101 controlled fluid flow inferred from hydrothermal vents imaged in 3D seismic reflection data, offshore
1102 NW Australia. *Basin Research*, **28**, 299-318, <http://doi.org/10.1111/bre.12111>.

1103
1104 Mannie, A.S., Jackson, C.A.L. & Hampson, G.J. 2014. Structural controls on the stratigraphic
1105 architecture of net-transgressive shallow-marine strata in a salt-influenced rift basin: Middle-to-Upper

- 1106 Jurassic Egersund Basin, Norwegian North Sea. *Basin Research*, **26**, 675-700,
1107 <http://doi.org/10.1111/bre.12058>.
- 1108
1109 Mannie, A.S., Jackson, C.A.L., Hampson, G.J. & Fraser, A.J. 2016. Tectonic controls on the spatial
1110 distribution and stratigraphic architecture of a net-transgressive shallow-marine synrift succession in a
1111 salt-influenced rift basin: Middle to Upper Jurassic, Norwegian Central North Sea. *Journal of the*
1112 *Geological Society*, **173**, 901-915, <http://doi.org/10.1144/jgs2016-033>.
- 1113
1114 Marcon, Y., Ondreas, H., Sahling, H., Bohrmann, G. & Olu, K. 2014. Fluid flow regimes and growth
1115 of a giant pockmark. *Geology*, **42**, 63-66, <http://doi.org/10.1130/g34801.1>.
- 1116
1117 McKie, T. & Williams, B. 2009. Triassic palaeogeography and fluvial dispersal across the northwest
1118 European Basins. *Geological Journal*, **44**, 711-741, <http://doi.org/10.1002/gj.1201>.
- 1119
1120 Michelsen, O., Nielsen, L.H., Johannessen, P.N., Andsbjerg, J. & Surlyk, F. 2003. The Jurassic of
1121 Denmark and Greenland: Jurassic lithostratigraphy and stratigraphic development onshore and
1122 offshore Denmark.
- 1123
1124 Mogensen, T.E. & Jensen, L.N. 1994. Cretaceous subsidence and inversion along the Tornquist Zone
1125 from Kattegat to the Egersund Basin. *First Break*, **12**, 211-222.
- 1126
1127 Mogensen, T.E. & Korstgård, J.A. 2003. Triassic and Jurassic transtension along part of the
1128 Sorgenfrei-Tornquist Zone in the Danish Kattegat. *Geological Survey of Denmark and Greenland*
1129 *Bulletin*, **1**, 439-458.
- 1130
1131 Montgomery, S.L. 1996. Cotton Valley lime pinnacle reef play: Branton Field. *AAPG Bulletin*, **80**,
1132 617-629.
- 1133
1134 Moore, C.H. 2001. *Carbonate reservoirs: porosity, evolution and diagenesis in a sequence*
1135 *stratigraphic framework*. Elsevier.
- 1136
1137 Nielsen, L.H. 2003. Late Triassic–Jurassic development of the Danish Basin and the Fennoscandian
1138 Border Zone, southern Scandinavia. *The Jurassic of Denmark and Greenland. Geological Survey of*
1139 *Denmark and Greenland Bulletin*, **1**, 459-526.
- 1140
1141 Olivarius, M. & Nielsen, L.H. 2016. Triassic paleogeography of the greater eastern Norwegian-
1142 Danish Basin: Constraints from provenance analysis of the Skagerrak Formation. *Marine and*
1143 *Petroleum Geology*, **69**, 168-182, <http://doi.org/http://dx.doi.org/10.1016/j.marpetgeo.2015.10.008>.
- 1144
1145 Otvos, E.G. 2000. Beach ridges—definitions and significance. *Geomorphology*, **32**, 83-108.
- 1146
1147 Patruno, S., Hampson, G.J. & Jackson, C.A.L. 2015a. Quantitative characterisation of deltaic and
1148 subaqueous clinofolds. *Earth-Science Reviews*, **142**, 79-119,
1149 <http://doi.org/http://dx.doi.org/10.1016/j.earscirev.2015.01.004>.
- 1150

- 1151 Patruno, S., Hampson, G.J., Jackson, C.A.L. & Dreyer, T. 2015b. Clinoform geometry,
1152 geomorphology, facies character and stratigraphic architecture of a sand-rich subaqueous delta:
1153 Jurassic Sognefjord Formation, offshore Norway. *Sedimentology*, **62**, 350-388,
1154 <http://doi.org/10.1111/sed.12153>.
- 1155
1156 Petersen, H., Nielsen, L., Bojesen-Koefoed, J.A., Mathiesen, A., Kristensen, L. & Dalhoff, F. 2008.
1157 Evaluation of the quality, thermal maturity and distribution of potential source rocks in the Danish
1158 part of the Norwegian–Danish Basin. *Geological Survey of Denmark and Greenland Bulletin*, **16**, 1-
1159 27.
- 1160
1161 Phillips, T.B., Jackson, C.A.L., Bell, R.E. & Duffy, O.B. 2018. Oblique reactivation of lithosphere-
1162 scale lineaments controls rift physiography – the upper-crustal expression of the Sorgenfrei–Tornquist
1163 Zone, offshore southern Norway. *Solid Earth*, **9**, 403-429, <http://doi.org/10.5194/se-9-403-2018>.
- 1164
1165 Phillips, T.B., Jackson, C.A.L., Bell, R.E., Duffy, O.B. & Fossen, H. 2016. Reactivation of
1166 intrabasement structures during rifting: A case study from offshore southern Norway. *Journal of*
1167 *Structural Geology*, **91**, 54-73, <http://doi.org/http://dx.doi.org/10.1016/j.jsg.2016.08.008>.
- 1168
1169 Posamentier, H. & Laurin, P. 2005. Seismic geomorphology of oligocene to miocene carbonate
1170 buildups offshore Madura, Indonesia *SEG Technical Program Expanded Abstracts 2005*. Society of
1171 Exploration Geophysicists, 429-431.
- 1172
1173 Posamentier, H.W. 2004. Seismic geomorphology: imaging elements of depositional systems from
1174 shelf to deep basin using 3D seismic data: implications for exploration and development. *Geological*
1175 *Society, London, Memoirs*, **29**, 11-24.
- 1176
1177 Posamentier, H.W. & Kolla, V. 2003. Seismic geomorphology and stratigraphy of depositional
1178 elements in deep-water settings. *Journal of Sedimentary Research*, **73**, 367-388.
- 1179
1180 Prélat, A., Hodgson, D.M. & Flint, S.S. 2009. Evolution, architecture and hierarchy of distributary
1181 deep-water deposits: a high-resolution outcrop investigation from the Permian Karoo Basin, South
1182 Africa. *Sedimentology*, **56**, 2132-2154, <http://doi.org/10.1111/j.1365-3091.2009.01073.x>.
- 1183
1184 Purkis, S., Casini, G., Hunt, D. & Colpaert, A. 2015. Morphometric patterns in Modern carbonate
1185 platforms can be applied to the ancient rock record: Similarities between Modern Alacranes Reef and
1186 Upper Palaeozoic platforms of the Barents Sea. *Sedimentary Geology*, **321**, 49-69,
1187 <http://doi.org/http://dx.doi.org/10.1016/j.sedgeo.2015.03.001>.
- 1188
1189 Rattey, R.P. & Hayward, A.B. 1993. Sequence Stratigraphy of a Failed Rift System - the Middle
1190 Jurassic to Early Cretaceous Basin Evolution of the Central and Northern North-Sea. *Petroleum*
1191 *Geology of Northwest Europe: Proceedings of the 4th Conference*, **4**, 215-249, <http://doi.org/Doi>
1192 [10.1144/0040215](http://doi.org/10.1144/0040215).
- 1193
1194 Rise, L., Bøe, R., Ottesen, D., Longva, O. & Olsen, H.A. 2008. Postglacial depositional environments
1195 and sedimentation rates in the Norwegian Channel off southern Norway. *Marine Geology*, **251**, 124-
1196 138, <http://doi.org/https://doi.org/10.1016/j.margeo.2008.02.012>.
- 1197

- 1198 Romans, B.W., Fildani, A., Hubbard, S.M., Covault, J.A., Fosdick, J.C. & Graham, S.A. 2011.
1199 Evolution of deep-water stratigraphic architecture, Magallanes Basin, Chile. *Marine and Petroleum*
1200 *Geology*, **28**, 612-628, <http://doi.org/https://doi.org/10.1016/j.marpetgeo.2010.05.002>.
- 1201
1202 Rosleff-Soerensen, B., Reuning, L., Back, S. & Kukla, P. 2012. Seismic geomorphology and growth
1203 architecture of a Miocene barrier reef, Browse Basin, NW-Australia. *Marine and Petroleum Geology*,
1204 **29**, 233-254, <http://doi.org/https://doi.org/10.1016/j.marpetgeo.2010.11.001>.
- 1205
1206 Ruf, A., Simo, J.A. & Hughes, T.M. 2008. Quantitative Characterization of Oligocene-Miocene
1207 Carbonate Mound Morphology from 3D Seismic Data: Applications to Geologic Modeling, East Java
1208 Basin, Indonesia. International Petroleum Technology Conference.
- 1209
1210 Ryseth, A., Fjellbirkeland, H., Osmundsen, I.K., Skålnes, Å. & Zachariassen, E. 1998. High-
1211 resolution stratigraphy and seismic attribute mapping of a fluvial reservoir: Middle Jurassic Ness
1212 Formation, Oseberg Field. *AAPG Bulletin*, **82**, 1627-1651.
- 1213
1214 Saller, A., Werner, K., Sugiaman, F., Cebastian, A., May, R., Glenn, D. & Barker, C. 2008.
1215 Characteristics of Pleistocene deep-water fan lobes and their application to an upper Miocene
1216 reservoir model, offshore East Kalimantan, Indonesia. *AAPG Bulletin*, **92**, 919.
- 1217
1218 Saqab, M.M. & Bourget, J. 2016. Seismic geomorphology and evolution of early-mid Miocene
1219 isolated carbonate build-ups in the Timor Sea, North West Shelf of Australia. *Marine Geology*, **379**,
1220 224-245, <http://doi.org/http://dx.doi.org/10.1016/j.margeo.2016.06.007>.
- 1221
1222 Schlager, W. 1981. The paradox of drowned reefs and carbonate platforms. *Geological Society of*
1223 *America Bulletin*, **92**, 197.
- 1224
1225 Schlager, W. 2000. Sedimentation rates and growth potential of tropical, cool-water and mud-mound
1226 carbonate systems. *Geological Society, London, Special Publications*, **178**, 217-227,
1227 <http://doi.org/10.1144/gsl.sp.2000.178.01.14>.
- 1228
1229 Skjerven, J., Rijs, F. & Kalheim, J. 1983. Late Palaeozoic to Early Cenozoic structural development
1230 of the south-southeastern Norwegian North Sea. *Petroleum Geology of the Southeastern North Sea*
1231 *and the Adjacent Onshore Areas*. Springer, 35-45.
- 1232
1233 Slatt, R.M. 2006. *Stratigraphic reservoir characterization for petroleum geologists, geophysicists,*
1234 *and engineers*. Elsevier.
- 1235
1236 Somme, T.O., Martinsen, O.J. & Lunt, I. 2013. Linking offshore stratigraphy to onshore
1237 paleotopography: The Late Jurassic-Paleocene evolution of the south Norwegian margin. *Geological*
1238 *Society of America Bulletin*, **125**, 1164-1186, <http://doi.org/10.1130/b30747.1>.
- 1239
1240 Sørensen, S. & Tangen, O.H. 1995. Exploration trends in marginal basins from Skagerrak to Stord. *In:*
1241 Hanslien, S. (ed) *Norwegian Petroleum Society Special Publications*. Elsevier, **Volume 4**, 97-114.
- 1242

- 1243 Sørensen, S., Morizot, H. & Skottheim, S. 1992. A tectonostratigraphic analysis of the southeast
1244 Northern North Sea Basin. In: Larsen, R.M., Brekke, H., Larsen, B.T. & Talleraas, E. (eds) *Structural*
1245 *and Tectonic modelling and its application to Petroleum Geology*. Elsevier, Amsterdam, **1**, 19-42.
- 1246
1247 Stewart, S. 1999. Seismic interpretation of circular geological structures. *Petroleum Geoscience*, **5**,
1248 273-285.
- 1249
1250 Thybo, H. 2000. Crustal structure and tectonic evolution of the Tornquist Fan region as revealed by
1251 geophysical methods. *Bulletin of the Geological Society of Denmark*, **46**, 145-160.
- 1252
1253 Tvedt, A.B.M., Rotevatn, A., Jackson, C.A.L., Fossen, H. & Gawthorpe, R.L. 2013. Growth of
1254 normal faults in multilayer sequences: A 3D seismic case study from the Egersund Basin, Norwegian
1255 North Sea. *Journal of Structural Geology*, **55**, 1-20, <http://doi.org/10.1016/j.jsg.2013.08.002>.
- 1256
1257 Underhill, J.R. & Partington, M.A. 1993. Jurassic thermal doming and deflation in the North Sea:
1258 implications of the sequence stratigraphic evidence. 337-345, <http://doi.org/10.1144/0040337>.
- 1259
1260 Vail, P.R. & Todd, R.G. 1981. Northern North Sea Jurassic unconformities, chronostratigraphy and
1261 sea-level changes from seismic stratigraphy. *Petroleum geology of the continental shelf of north-west*
1262 *Europe*. Heyden, London, 216-235.
- 1263
1264 Van Der Zwaan, G.J. & Jorissen, F.J. 1991. Biofacial patterns in river-induced shelf anoxia.
1265 *Geological Society, London, Special Publications*, **58**, 65.
- 1266
1267 van Wees, J.D., Stephenson, R.A., Ziegler, P.A., Bayer, U., McCann, T., Dadlez, R., Gaupp, R.,
1268 Narkiewicz, M., *et al.* 2000. On the origin of the Southern Permian Basin, Central Europe. *Marine*
1269 *and Petroleum Geology*, **17**, 43-59, [http://doi.org/http://dx.doi.org/10.1016/S0264-8172\(99\)00052-5](http://doi.org/http://dx.doi.org/10.1016/S0264-8172(99)00052-5).
- 1270
1271 Vespremeanu-Stroe, A., Preoteasa, L., Zăinescu, F., Rotaru, S., Croitoru, L. & Timar-Gabor, A. 2016.
1272 Formation of Danube delta beach ridge plains and signatures in morphology. *Quaternary*
1273 *International*, **415**, 268-285, <http://doi.org/http://dx.doi.org/10.1016/j.quaint.2015.12.060>.
- 1274
1275 Vollset, J. & Doré, A.G. 1984. A revised Triassic and Jurassic lithostratigraphic nomenclature for the
1276 Norwegian North Sea. *Norwegian Petroleum Directorate, Bull.*, **3**, 1-51.
- 1277
1278 Widess, M.B. 1973. How thin is a thin bed? *GEOPHYSICS*, **38**, 1176-1180,
1279 <http://doi.org/10.1190/1.1440403>.
- 1280
1281 Zhang, J.-J., Wu, S.-H., Fan, T.-E., Fan, H.-J., Jiang, L., Chen, C., Wu, Q.-Y. & Lin, P. 2016.
1282 Research on the architecture of submarine-fan lobes in the Niger Delta Basin, offshore West Africa.
1283 *Journal of Palaeogeography*, **5**, 185-204, <http://doi.org/http://dx.doi.org/10.1016/j.jop.2016.05.005>.
- 1284
1285 Zhuo, H., Wang, Y., Shi, H., Zhu, M., He, M., Chen, W. & Li, H. 2014. Seismic geomorphology,
1286 architecture and genesis of Miocene shelf sand ridges in the Pearl River Mouth Basin, northern South
1287 China Sea. *Marine and Petroleum Geology*, **54**, 106-122,
1288 <http://doi.org/http://dx.doi.org/10.1016/j.marpetgeo.2014.03.002>.

1289

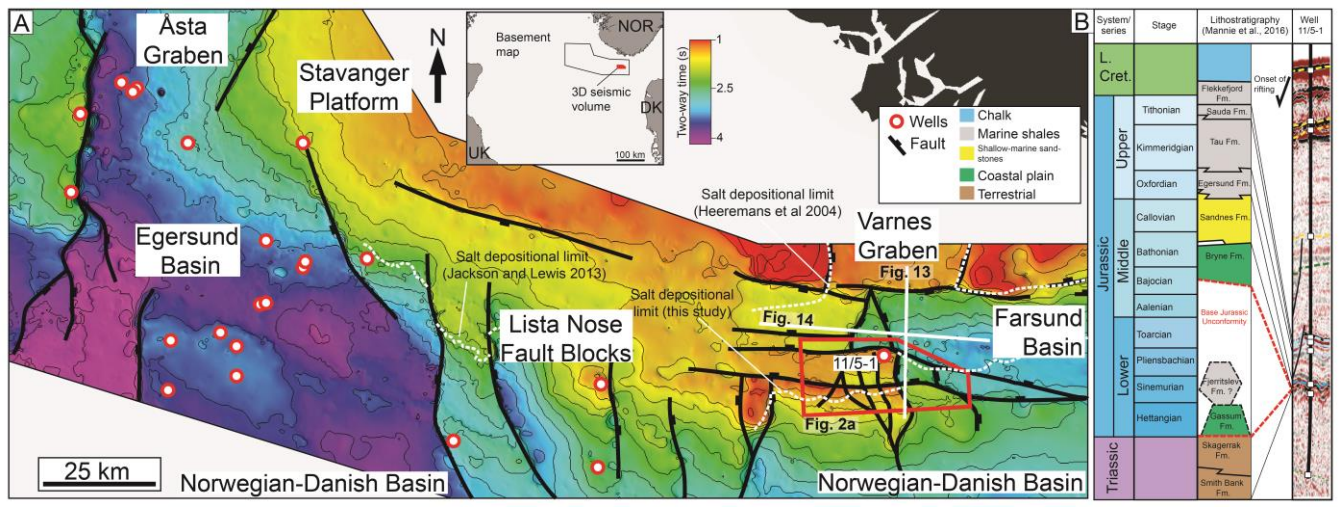
1290 Ziegler, P.A. 1992. North Sea Rift System. *Tectonophysics*, **208**, 55-75.

1291

1292

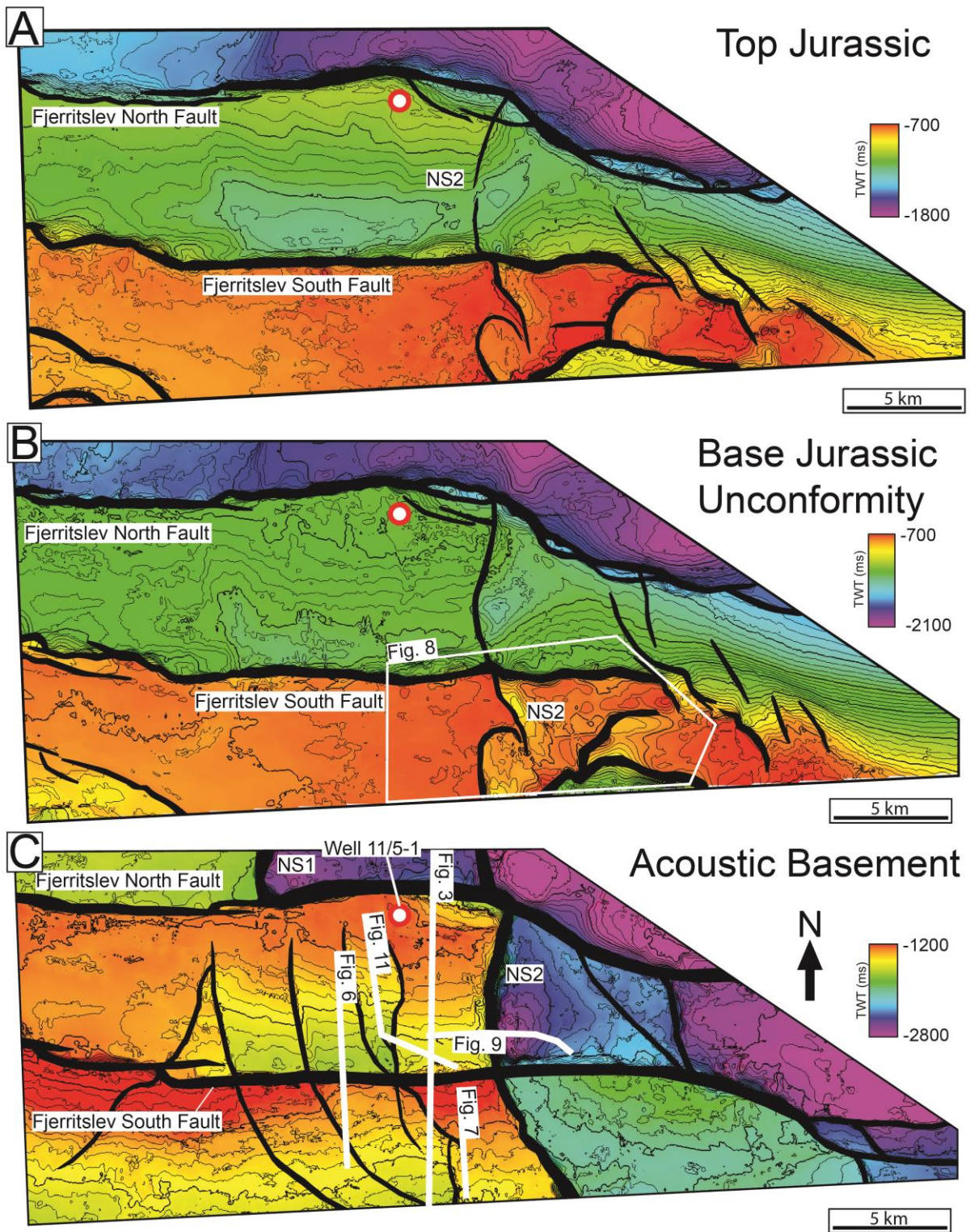
1293 **Figure 1**

1294

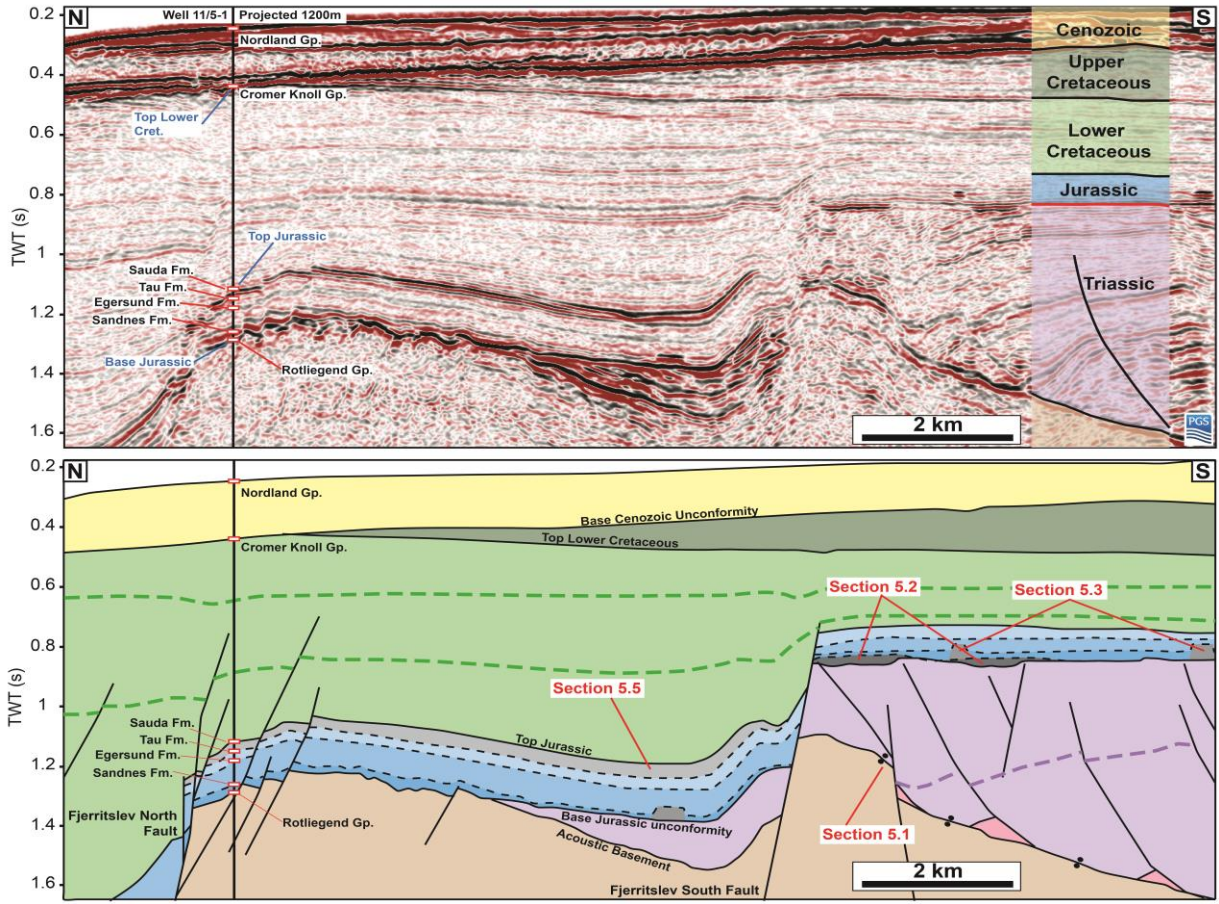


1295

1296

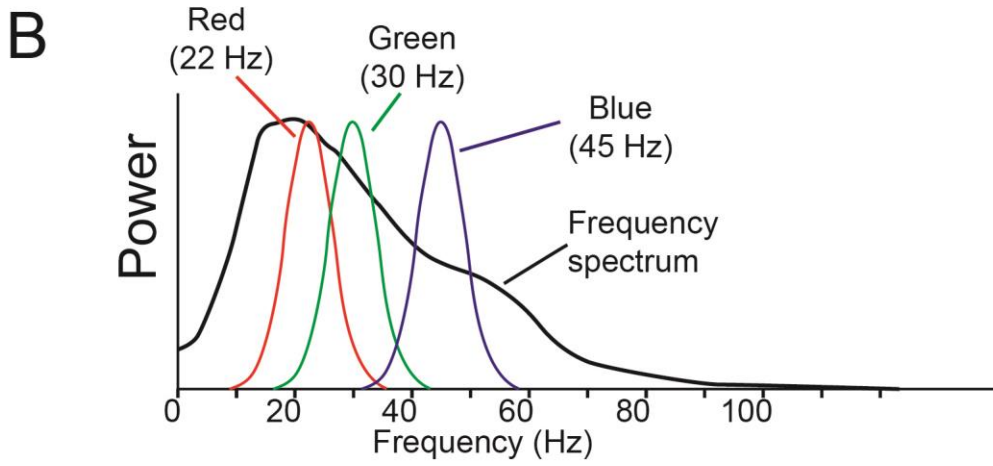
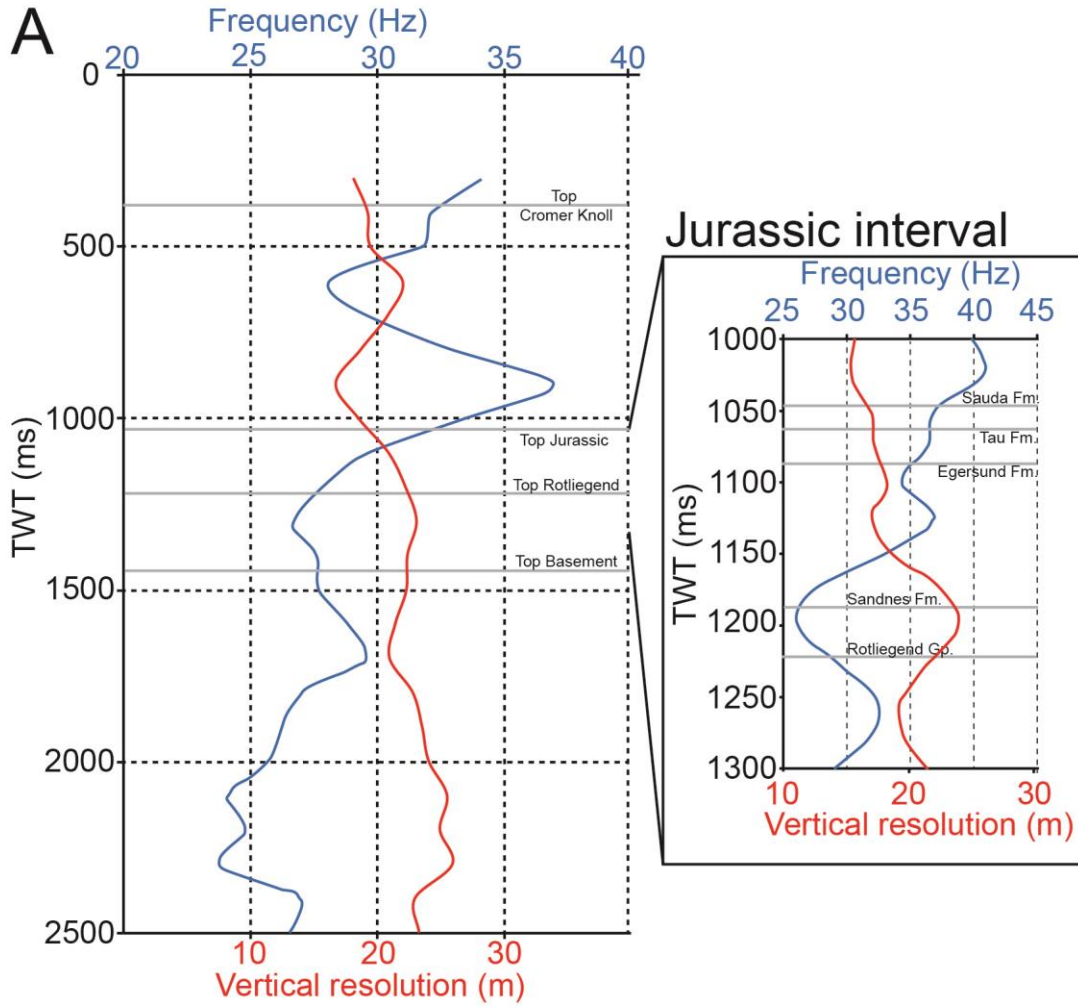


1300 **Figure 3**

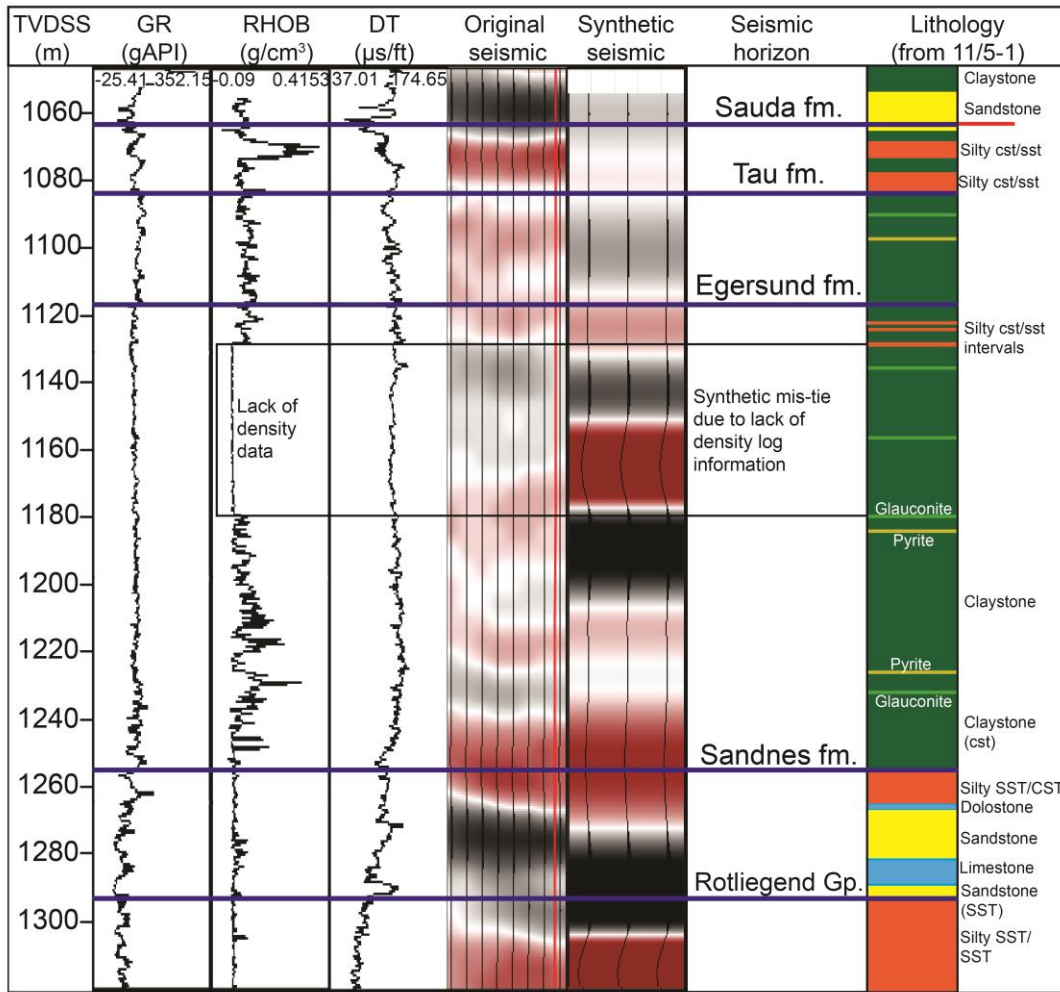


1301

1302



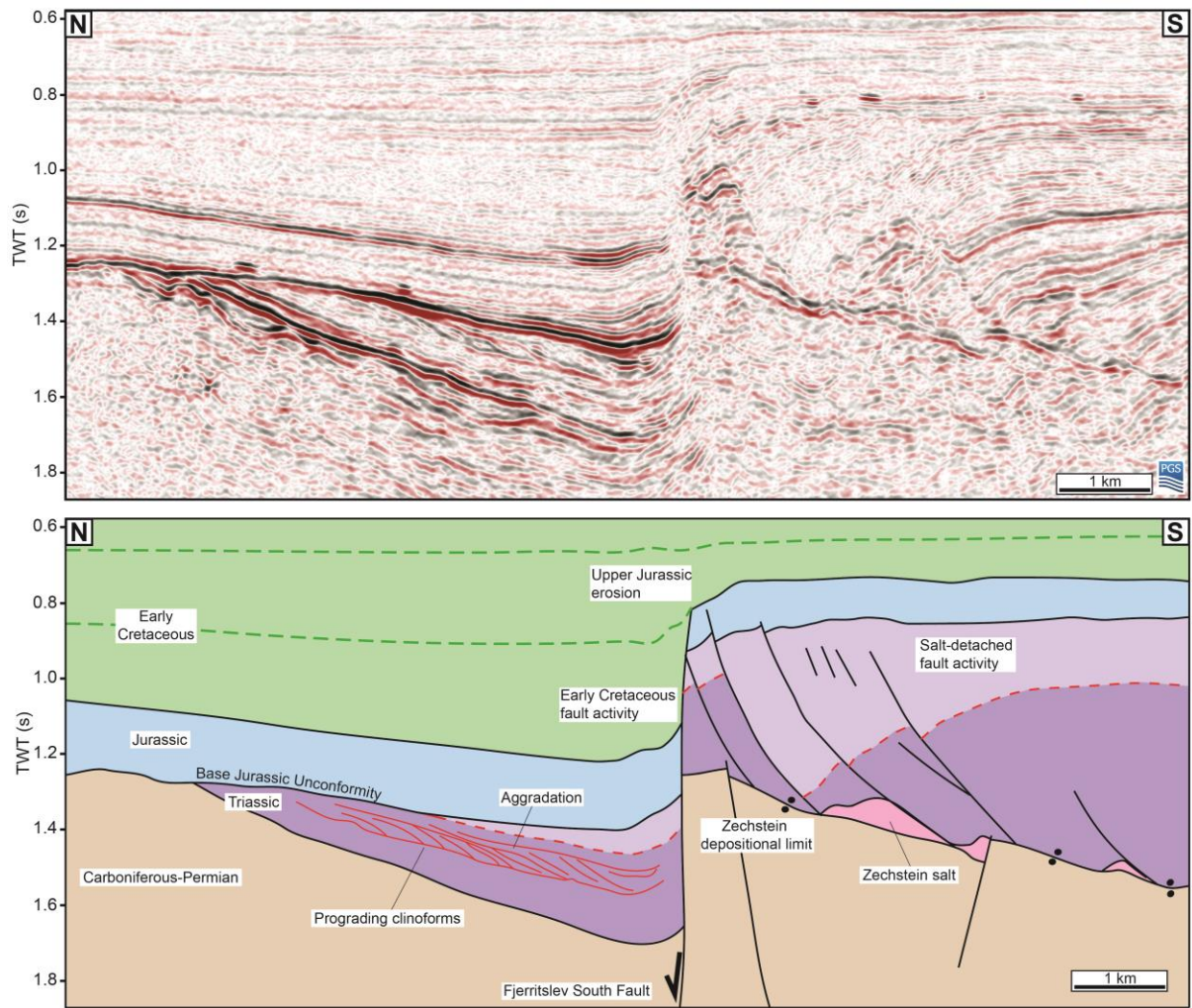
1306 **Figure 5**



1307

1308

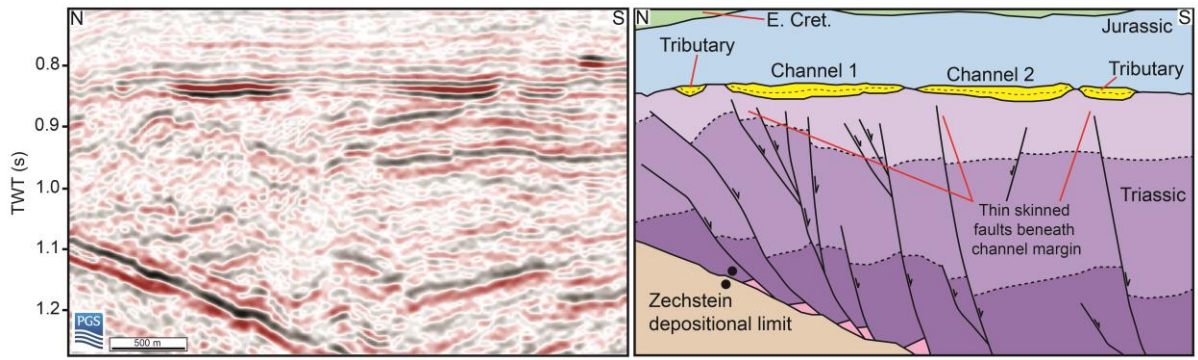
1309 **Figure 6**



1310

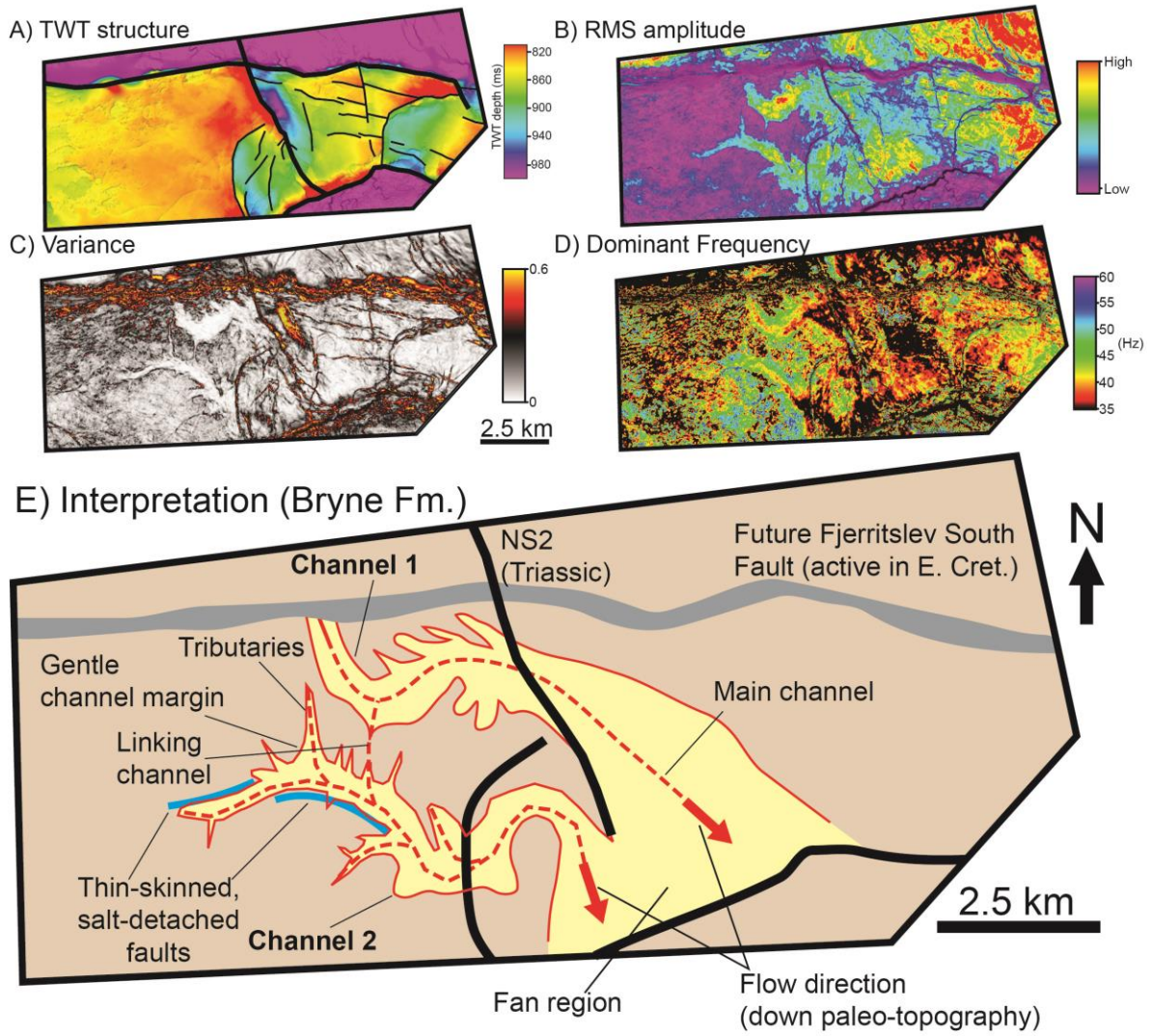
1311

1312 **Figure 7**

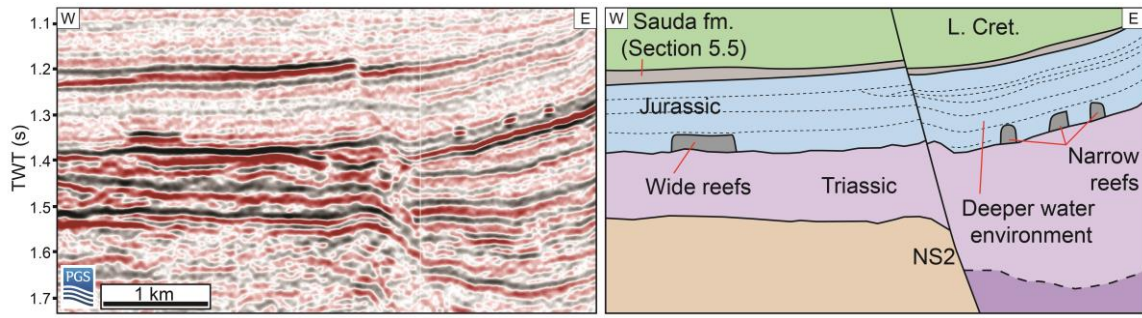


1313

1314



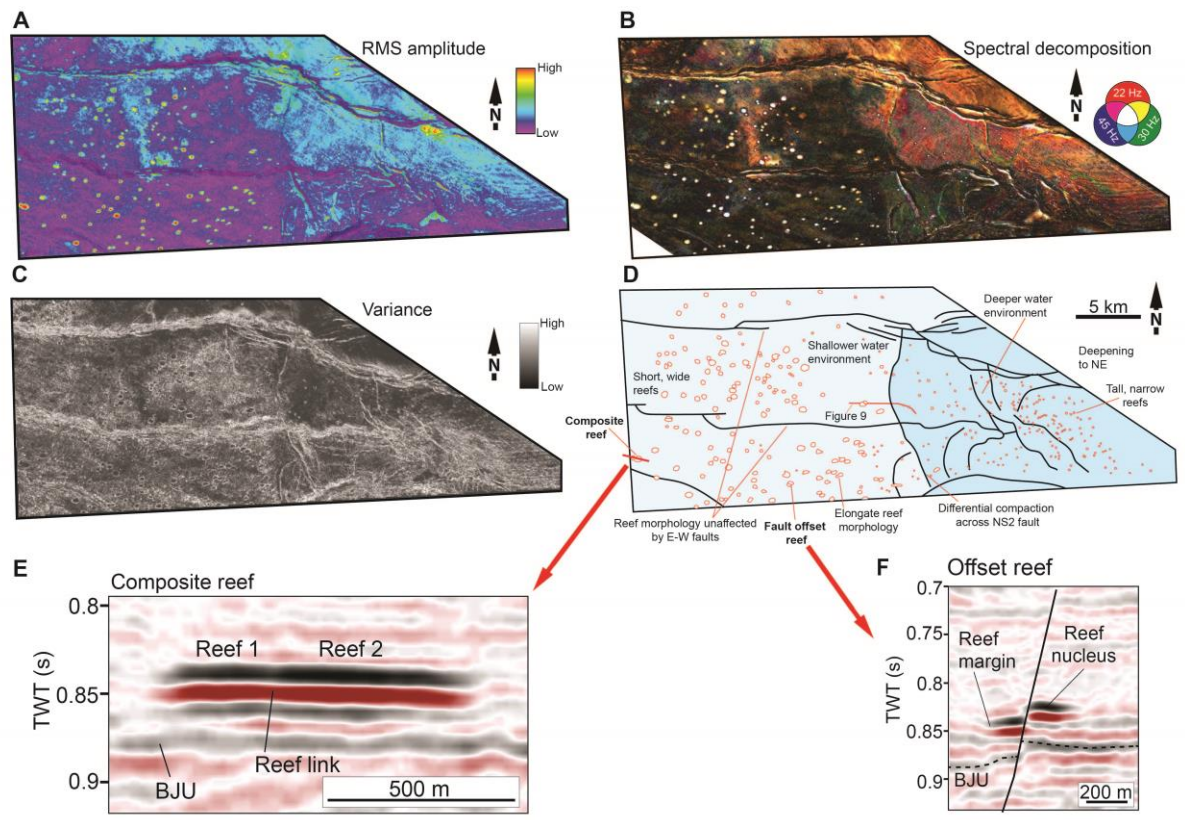
1318 **Figure 9**



1319

1320

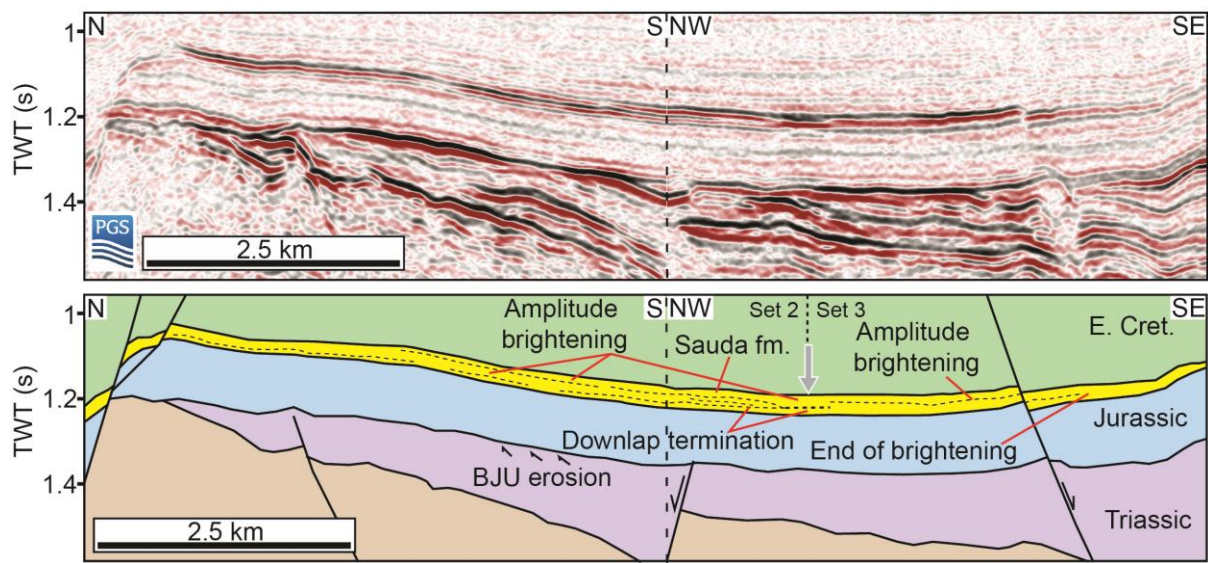
1321 **Figure 10**



1322

1323

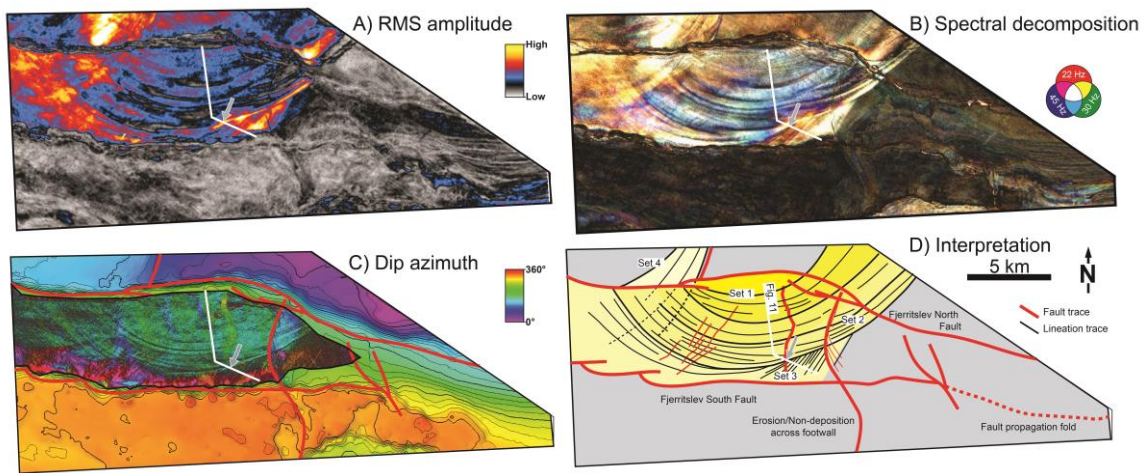
1324 **Figure 11**



1325

1326

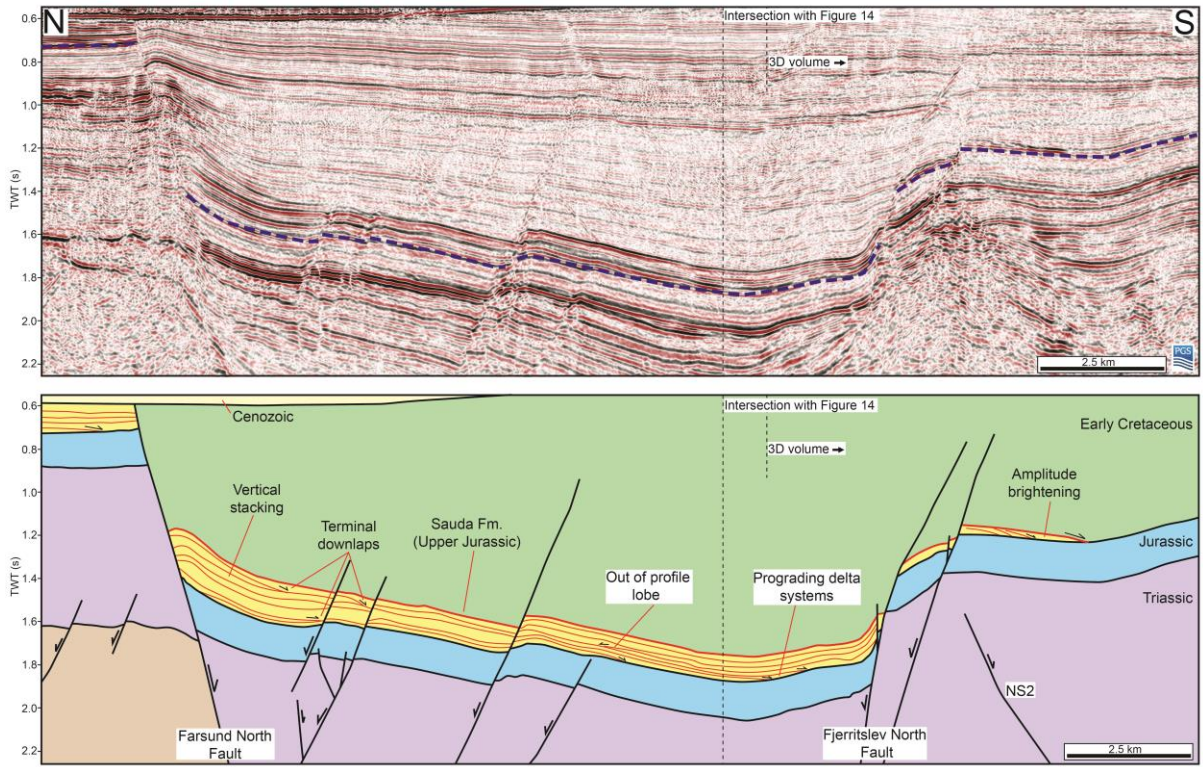
1327 **Figure 12**



1328

1329

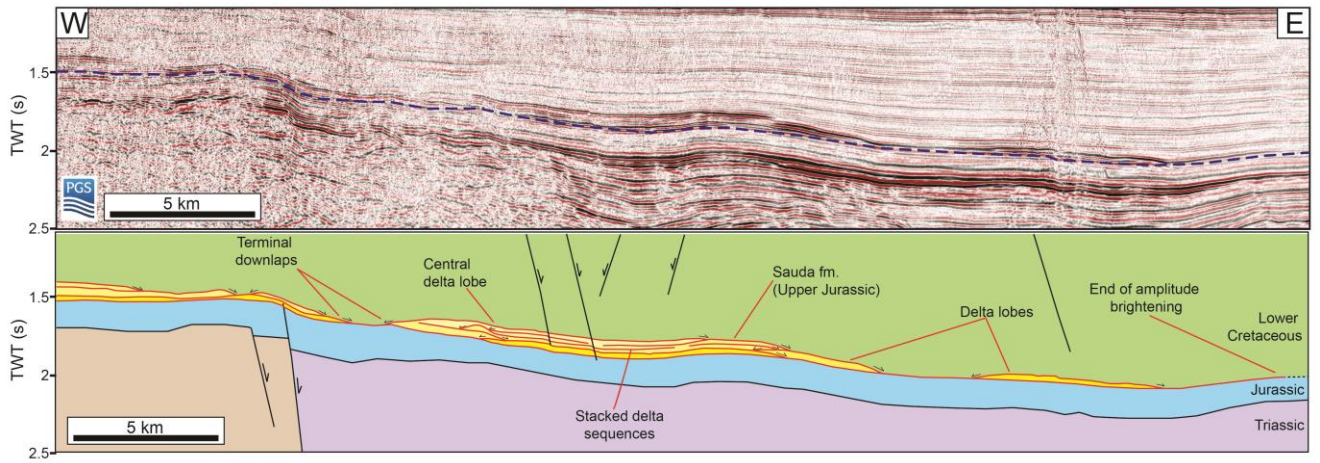
1330 **Figure 13**



1331

1332

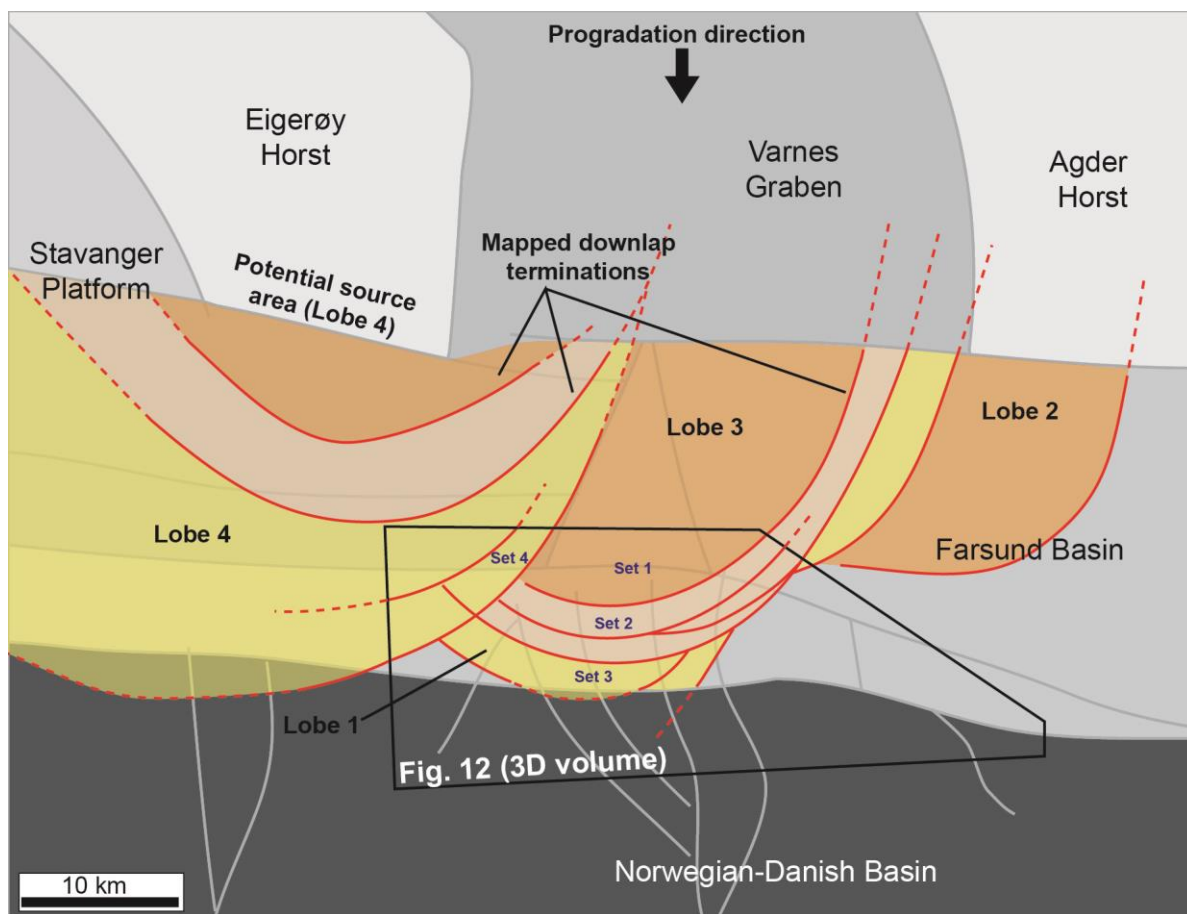
1333 **Figure 14**



1334

1335

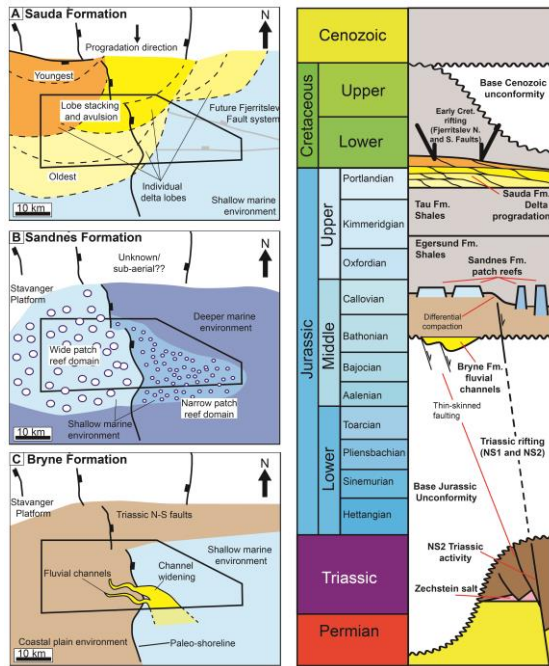
1336 **Figure 15**



1337

1338

Figure 16

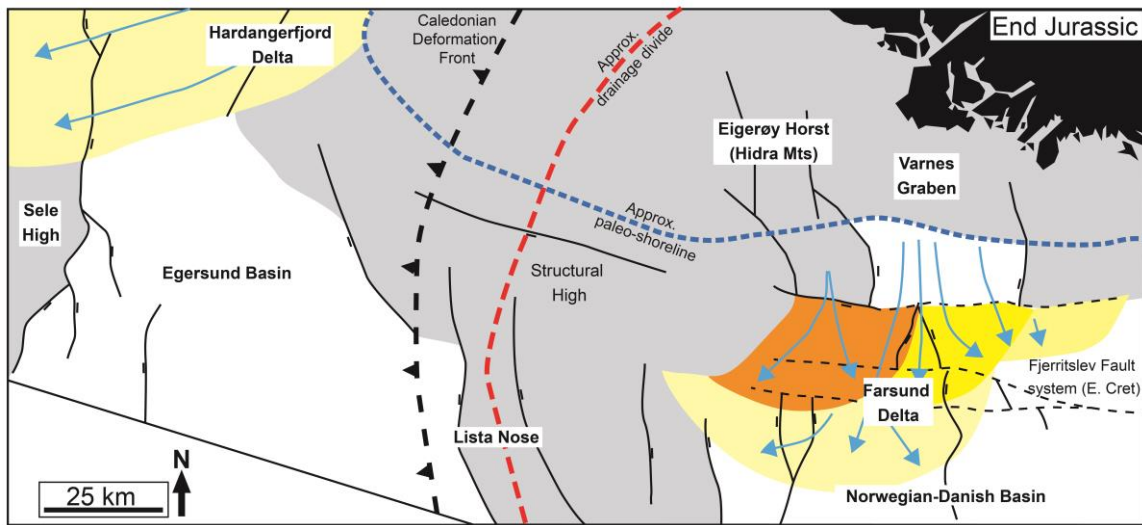


1340

1341

1342

1343 **Figure 17**



1344